NTNU – Trondheim
Norwegian University of
Science and Technology

Evaluation of Magnetic Leakage Field and the Need for Screening with Respect to Induction Power Transfer (IPT) System

Jon-Inge Venvik

Master of Science in Electric Power Engineering
Submission date: June 2014
Supervisor: Arne Nysveen, ELKRAFT
Co-supervisor: Giuseppe Guidi, SINTEF Energy Research

Norwegian University of Science and Technology
Department of Electric Power Engineering

Evaluation of magnetic leakage field and the Need for Shielding with respect to Induction Power Transfer (IPT) System

Problem description

Technology for wireless, inductive, battery charging has the potential to enable new applications of electric transportation. In particular, inductive power transfer for battery powered ships is a new application currently under investigation in a research project managed by Wärtsilä Norway. For such ships, inductive power transfer can ensure full utilization of the docking time for charging, and thereby help to reduce the required size of the battery. Thus, an automated wireless system with high power transfer capability under harsh environmental conditions is required. The scope of this project is to look in to the time-varying magnetic field created by this system and perform studies on how it complies with safety and regulations.

More specifically the objective is to:

- Develop methods and models for computing electromagnetic leakage field.
- Evaluate the need for shielding.
- Perform measurements on magnetic fields created by coils energized with a current.
- Compare measurements with FEM analysis.

Summary

This report considers a system for transferring electric power from shore to ships for charging of electrical driven ferries by use of induction power transfer (IPT). The IPT works by leading an alternating current through a coil stationed on shore which creates a time-varying magnetic field. This magnetic field will, through an air gap induce a voltage in another coil stationed on a ship, making it possible to transfer power wirelessly by means of induction.

The IPT system will, as well as transferring power to the receiving coil also produce a time-varying magnetic field in the nearby surroundings which practically can be considered a leakage field, but can to some extent also be defined as electromagnetic radiation.

In Norway, regulations regarding both ionizing and non-ionizing radiation are given by the Norwegian Radiation Protection Authority (NRPA). The IPT system operates in frequencies from 3 – 5 kHz and therefore the magnetic leakage field is considered as non-ionizing radiation. Requirements given by NRPA do not say anything specific about permitted levels of magnetic field strength because the energy absorbed by the body varies with frequency. Generally the NRPA says that the magnetic leakage field should be kept as low as practically possible and refer to reference levels given in guidelines published by the International Commission on Non-Ionizing Radiation Protection (ICNIRP).

To obtain an overview of the radiation created by the IPT and how it complies with the reference levels, the IPT system is modelled in COMSOL Multiphysics with one specific configuration of the coils and the current. The simulations have shown that the IPT will create time-varying magnetic fields that cause radiation above reference levels given in the ICNIRP guidelines; however the effect to the surroundings can be significantly reduced by use of shielding such as aluminum plates in various configurations.

The method used for modelling the IPT system has been verified by modelling an actual coil found in storage at SINTEF Energy research. This coil had been energized with a current of 10A and the magnetic flux density created by the energized coil has been measured and compared with COMSOL simulations.

Sammendrag

Denne prosjektrapporten tar for seg et system ved bruk av induksjon overfører elektrisk energi *(Induction Power Transfer, IPT)* fra landanlegg til skip, i dette tilfellet for å lade batteriene i elektrisk drevne ferger. Systemet fungerer på en slik måte at en vekselstrøm som føres gjennom en spole stasjonert på landsiden vil skape et tidsvarierende magnetfelt som i sin tur vil indusere en spenning i en mottakerspole montert på fergen. Dette gjør det mulig å overføre elektrisk energi trådløst ved induksjon.

Dette systemet vil, i tillegg til å overføre elektrisk energi til en mottakerspole også skape et tidsvarierende magnetisk felt som lekker ut til nærliggende område, hvilket også til en viss grad kan karakteriseres som elektromagnetisk stråling.

I Norge er det Statens Strålevern som utgir forskrifter som omhandler både ioniserende og ikke-ioniserende stråling. IPT-systemet opererer i et frekvensområde fra 3 – 5 kHz og magnetfeltet kan derfor karakteriseres som ikke-ioniserende stråling. Strålevernet kommer ikke med noen spesifikke krav til høyest tillatt magnetisk feltstyrke da energien som absorberes i kroppen avhenger av frekvens. Generelt sier Strålevernet at strålingen skal holdes så lav som mulig og referer til referanseverdier som er gitt i retningslinjer publisert av Den Internasjonale Kommisjon for Beskyttelse mot Ikke-Ioniserende Stråling (ICNIRP).

For å få en oversikt over strålingen som skapes av IPT systemet og hvordan det svarer til forskriftene er hele systemet modellert i COMSOL Multiphysics med én spesifikk konfigurasjon av spolen og strømmen. Simuleringene har vist at IPT-systemet vil skape et tidsvarierende magnetisk felt som medfører en stråling over de anbefalte verdiene i ICNIRP sine retningslinjer; men strålingens effekt på omgivelsene kan bli betydelig redusert ved bruk av skjerming.

Metoden som er brukt for å evaluere IPT systemet i COMSOL har blitt verifisert ved å modellere en annen spole som er funnet på SINTEF Energi sitt lager. Denne spolen har blitt modellert og simulert i COMSOL på samme måte som IPT systemet. Resultatene fra denne simuleringen er sammenlignet med målinger av det magnetiske feltet som er gjort når det er satt strøm på 10 A gjennom spolen.

Preface

This is a project report on the master thesis with subject TET4910 for the master program “MSc Electric power engineering” at Norwegian University of Science and Technology.

This project has done studies on electromagnetic fields and radiation of induction power transfer using a finite element method (FEM) software called COMSOL Multiphysics. It has further been made considerations on how the radiation levels comply with regulations. Through this project I have learned much of the opportunities with FEM software, but also that good result from simulations depends on prior knowledge.

I would like to thank my supervisor at NTNU, Professor Arne Nysveen as well as Niklas Magnusson and Giuseppe Guidi at SINTEF Energy research for their guidance through this project. My gratitude also goes to Lars Klæboe at Norwegian Radiation Protection Authority for his assistance.

Trondheim 11.06.14

Jon-Inge Venvik

Table of contents

List of figures

Abbreviations

- EMC – Electromagnetic compatibility
- EMF – Electromagnetic field
- NIR – Non-ionizing radiation
- SA – Specific energy absorption
- SAR – Specific energy absorption rate
- S – power density

1. Introduction

1.1. Background

Electric driven transportations has in the later times become more and more common as the world seeks to lower its energy costs and CO_2 emissions. In this context cars, busses and now also ferries are developing from carbon based combustion to electric driven propulsion by means of energy storage in batteries. In order to make charging effective there is an ongoing research to make it possible without using cables and having to connect and disconnect for every time. For charging large battery banks such as electric driven ferries this would be especially feasibly because a ferry has a short stay in dock, and the number of crew is always kept as limited as possible.

SINTEF Energy Research has on behalf of Wärtsilä in Norway an ongoing project where the subject is to come up with a good solution to transfer electric energy from shore to a ferry by use of induction power transfer (IPT). The principle is to apply a high frequency current to a sending coil which is located on the shore side. This will create a powerful magnetic field which will induce a voltage in a coil with the same physical size mounted on the ferry, which in turn is used for charging a battery through a rectifier. The project about IPT is more thoroughly described in the SINTEF report considering this project [1].

1.2. Problem description

One of the challenges by induction power transfer is that the magnetic field created by the coils will leak across a large area. This in combination with high frequency will cause low-frequency electromagnetic radiation that may be harmful to living tissue. Therefore it is necessary to do studies on the magnetic field related to the IPT in order to identify how strong and potentially hazardous it is. This must, in turn be weighed against rules and regulations which are typically based on research on radiation.

Measures to reduce the time-varying magnetic leakage field will also be investigated and considered with respect to effectiveness and costs.

2. Theory on electromagnetic fields and regulations

2.1. Basis for regulations

Former studies on time-varying magnetic field with Extremely Low Frequency (ELF) and Very Low Frequency (VLF) are mainly focused on the magnetic stray field produced by power lines. This stray field may be referred to as electromagnetic radiation, e.g. [2] or [3] or non-ionizing radiation [4].

The Norwegian Radiation Protection Authority (NRPA) does not provide specific limits for non-ionizing electromagnetic radiation at all frequencies, but § 34 in Norwegian regulations regarding exposure levels [5] say: *"All eksponering av mennesker for ikke-ioniserende stråling skal holdes så lav som praktisk mulig".* Translated in to English the regulation means that all human exposure to non-ionizing radiation should be kept as low as practically possible.

The Norwegian regulations are not conclusive on permitted EMC levels, but according to Lars Klæboe[1] in Norwegian Radiation Protection Authority (NRPA) they refer to studies such as "Guidelines for limiting exposure to time-varying electric, magnetic and electromagnetic fields" provided by the International Commission on Non-Ionizing Radiation Protection (ICNIRP) [6].

While electromagnetic fields produced by transformers and high-voltage power lines make non-ionizing radiation (NIR), ionizing radiation is produced from radioactive sources such as nuclear waste. The whole frequency spectrum is illustrated in Figure 2.1.

[1]E-mail correspondence with Lars Klæboe 30.04.14. Scientist in section for non-medical use of radiation, NRPA.

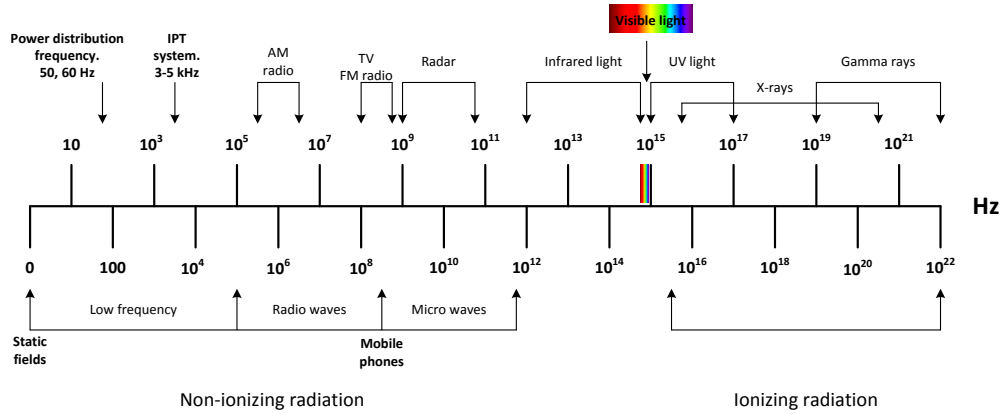

Figure 2.1 - Frequency spectrum.

2.2. Electromagnetic fields (EMF)

The expression *electromagnetic field* refers to the theory of electromagnetism that describes electric field, magnetic fields and the relationship between those. Briefly explained, a conductor with a high voltage difference to the surroundings will cause a strong electric field (E-field) and expressed as Volt per meter [V/m].

A conductor carrying a high current will cause a strong magnetic field which can be referred to as magnetic flux density [B], expressed in tesla [T], or as magnetic field strength, H expressed in ampere per meter [A/m], and the two terms are related by the expression:

$$B = \mu H \tag{2.1}$$

where μ equals the magnetic permeability for a material which for air and other non-magnetic materials is $4\pi \cdot 10^{-7}$ henry per meter [H/m].

Both H-field and E-field are given on vector form and can be considered to be mutually perpendicular as shown in Figure 2.2, and therefore H-field field may be computed by means of measuring the E-field. However, in the near-field region E and H are not proportional which makes it necessary to conduct direct measurements on the H-field. The basic methods for measuring H-field can be derived from Maxwell's equation saying that an alternating flux will induce a voltage:

$$U = -\frac{\partial \phi}{\partial t} \tag{2.2}$$

And

$$B = \frac{\phi}{A} \tag{2.3}$$

where ϕ is the total flux and A is the cross-section area of a material.

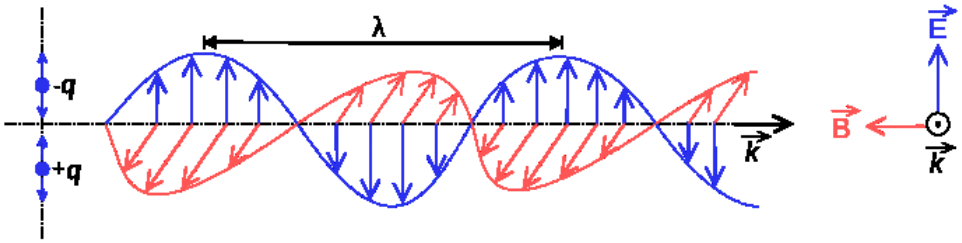

Figure 2.2 - Magnetic fields, B and electric fields, E goes perpendicular through space, *k*. [7]

2.3. Effect of EMF to a human body

There are two considerations that must be taken in to account when doing studies on EMF radiation; the short term effect which can be studied through experiments on volunteers, and the long term effect which requires studies over a longer period of time on people who are exposed to such fields.

Short term effect: There are three coupling mechanisms which directly relate time-varying electric and magnetic fields with tissue and living matter, [6];

- Coupling to low-frequency electric fields
- Coupling to low-frequency magnetic fields
- Absorption of energy from electromagnetic fields

Electric fields external to the body will induce surface charges on to the body resulting in induced currents inside the body as described in [6]. The magnitude of these surface charges depends on the shape of the body and the relative position the field, and the magnitude of the resulting currents flowing through the body depends on the body's electrical conductivity and permeability.

A time-varying magnetic field on the human body will result in induced electric fields and circulating currents through body tissue, and the magnitude of these

currents will depend on the radius of the loop, the electrical conductivity of the tissue and the rate of change of the magnetic field. Therefore exposure to electric and magnetic fields may affect cardiac functions and will also result in heating of body tissue, but it depends on the power density. Exposure to lower electric and magnetic fields normally results in negligible energy absorption and temperature increase within the body, but frequencies above 100 kHz can lead to significant temperature increase. The effect can be compared with a micro-wave oven.

In addition to the direct coupling mechanisms between electromagnetic fields and living matter there are also two indirect coupling mechanisms:

- Direct contact with an object at a different electric potential that will cause electric currents to through the body. E.g. if one holds on to a wire which obtains a potential difference in the endings due to voltage induction. The path of the electric currents through the body depends on the contact area of the body, but currents above 30 mA through heart and lounge may cause cardiac malfunction and is considered to be potentially lethal
- Coupling of EMF to medical devices.

Long term effect: There several studies on the long-term effect of being exposed to electromagnetic fields, including epidemiological studies on reproductive outcome as well as residential and occupational cancer studies, e.g. [8], [9] or [10]. These studies mainly focus on the effect of being close to high-voltage power lines and include laboratory studies as well as both occupational and volunteer studies. A lot of the studies focus on the cohesion of childhood cancer and exposure to power-frequency magnetic fields in homes caused by nearby power lines. There have been several indications that there might be a connection between the exposure to electromagnetic fields and different types of cancer, including leukemia with children.

2.4. Restrictions

The maximum permitted EMF radiation levels are decided by the Norwegian Radiation Protection Authority, but the regulations regarding time varying magnetic field only says that it shall not be of harm to human or animals. The exposure level limitations are differentiated between occupational population; adult people who are working under known conditions and trained to take precautions, and the general public which may consists of people with varying age and health status. The general public can neither expected to have knowledge of NIR or be aware of their exposure to EMF.

For the frequency range from 50 Hz to 100 kHz, the basic restrictions are derived from current density, J [A/m^2] within the body tissue, taken in to account that absorption of energy depends on the size of tissue and orientation to the field. Also reflection, focusing and scattering of the field can result in enhanced localized absorption of energy.

For the frequency range from 1-100 kHz the basic guidelines says that the maximum current density for head and trunk should not be more than *f/100* [mA/m^2] (rms), i.e. a 5 kHz field should not induce a current density of more than 5 mA/m^2 for occupational personnel. For the general public an additional safety factor of 5 applies; i.e. 1 mA/m^2. The models for magnetic fields assume a homogenous conductivity and apply simple circular conductive loop models to estimate induced currents in different body regions, where current density from a pure sinusoidal field with a frequency, f is derived from Faraday's induction law:

$$J = \pi R f \sigma B \tag{2.4}$$

If, according to [11] a homogenous conductivity in head and trunk of 0.2 S/m is assumed, a 60 Hz magnetic field with flux density of 100 µT would generate current densities between 0.2 and 2 mA/m^2 in the peripheral area of the body.

2.5. Reference levels with respect to magnetic flux density

The complete overview of reference levels regarding the occupational and general public exposure to time-varying electric and magnetic fields are given in the ICNIRP Guidelines. The guidelines published in 1997 [6] said that the reference levels for magnetic fields in the frequency range from 1 to 100 kHz should be kept below 6.25 µT$_{(RMS)}$ as shown in Figure 2.3. However, this was updated in 2010 [12] and now says that it should be below 27 µT $_{(RMS)}$ as shown in Figure 2.4.

The guidelines from the ICNIRP is the only report found that provides reference levels for a time varying magnetic field at all frequencies as given in figures Figure 2.3 and Figure 2.4. Note that the ICNIRP says that these are not absolute demands, but that additional measurements and evaluation regarding the magnetic field must be performed if the flux density turns out to be above recommended values in the guidelines.

The guidelines are also supported in other studies, e.g. [11].

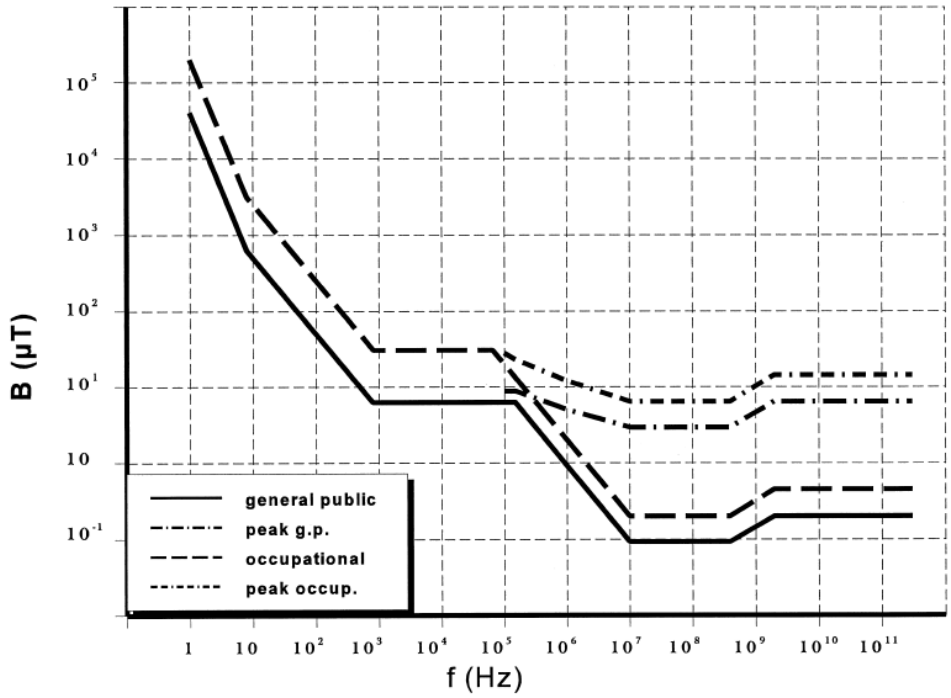

Figure 2.3 - "Reference levels for exposure to time varying magnetic fields" given in ICNIRP guidelines from 1997 [6].

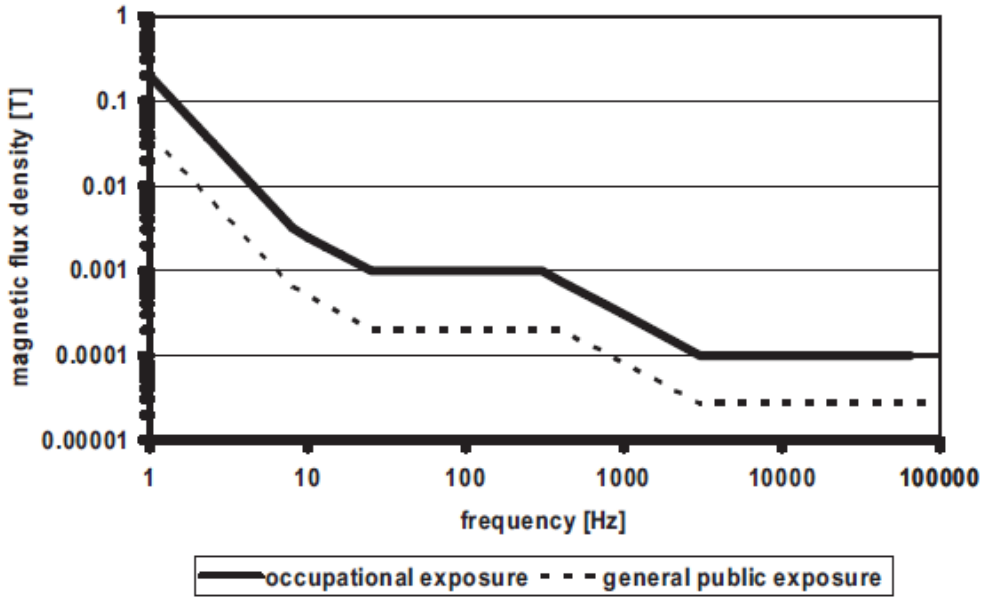

Figure 2.4 - "Reference levels for exposure to time varying magnetic fields" given in ICNIRP guidelines from 2010 [12].

3. Method for evaluation of magnetic field

3.1. Finite Element Method

Because of the complex geometry of the IPT system, it would be very time consuming to do analytical calculations in order to create an image in how the magnetic field produced by the IPT system forms. Finite element method (FEM) is according to [13] referred to in [14] defined as a numerical technique for finding solutions to mathematical differential equations. COMSOL Multiphysics [15] is a FEM-software that can be used for drawing geometry in 1D, 2D or 3D space and apply various materials and any kind of physics to the geometry. For this project, only studies on magnetic fields are performed.

3.1.1. 2D models with symmetrical axis

The simplest way of evaluating a magnetic field in COMSOL is to draw a 2D model as shown in Figure 3.1 with a central symmetry axis which is a quick and easy method. One drawback of this method is that it requires all coils to be circular and centered on the symmetry axis, which will make the FEM model unable to evaluate the actual shape of the IPT and misalignment between sending and receiving coil. However it should sufficient to give a close estimate within the same range as a full 3D evaluation considering the field, and also to differentiate between the various geometries.

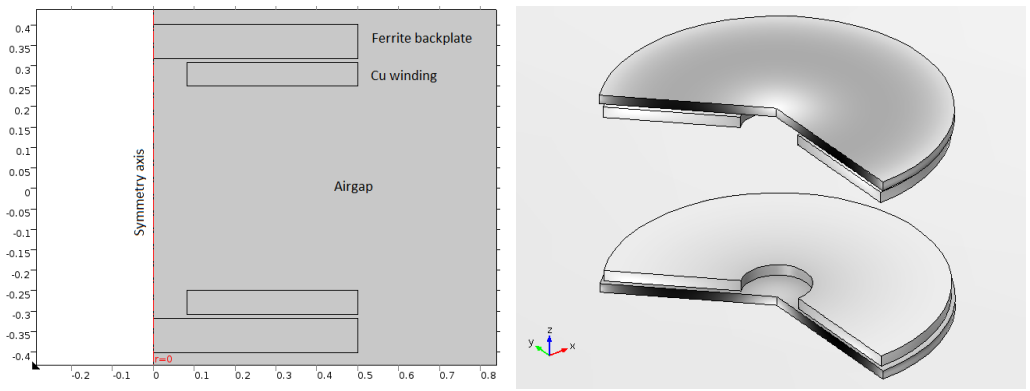

a b

Figure 3.1 – IPT system drawn with symmetry axis (a) and image on how COMSOL interprets the geometry (b)

3.1.2. 3D models with symmetry line

Doing computations on full-scale 3D models in FEM software such as COMSOL is likely to demand a lot of computational resources which in turn is time consuming. Therefore some simplifications can be done, such as drawing only one fourth of the model as shown in Figure 3.2, and applying boundaries with magnetic insulation using the expression; $n \times A = 0$. This will ensure that no flux lines cross the boundary which makes it possible to evaluate the field in the same way as a full scale model. The method is expected to work fine as long as sending and receiving end are aligned.

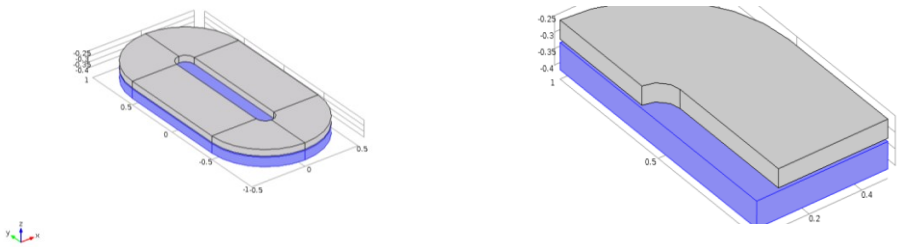

a *b*

Figure 3.2 - 3D model of sending end coil in the induction power transfer system where (a) is a complete scale model and (b) is a simplified model using lines of symmetry.

In order to test of the method, both geometries are now modelled with the same coil and the same current to verify that it is done correctly. The result is plotted in Figure 3.3 which shows that the method using magnetic insulation boundaries works well.

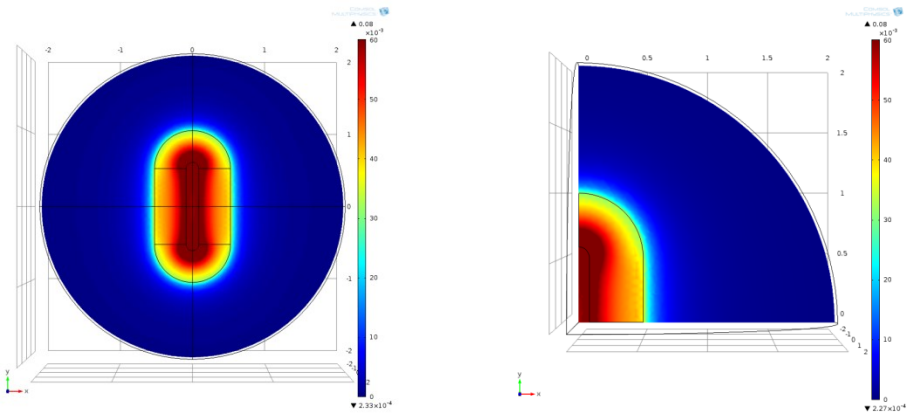

a b

Figure 3.3 - Plot of *magnetic flux density norm* comparing the full scale model (a) against the simplified model (b)

3.1.3. Full scale 3D model

To be able to do computations in the magnetic field and other aspects of the IPT system, a full scale 3D model must be made. This will make it possible to do the most accurate calculations on field with shielding applied and when the coils are not aligned. Figure 3.4 shows a drawing of a full scale 3D geometry of the sending and receiving end if the IPT, where numbers on the grid represents meters.

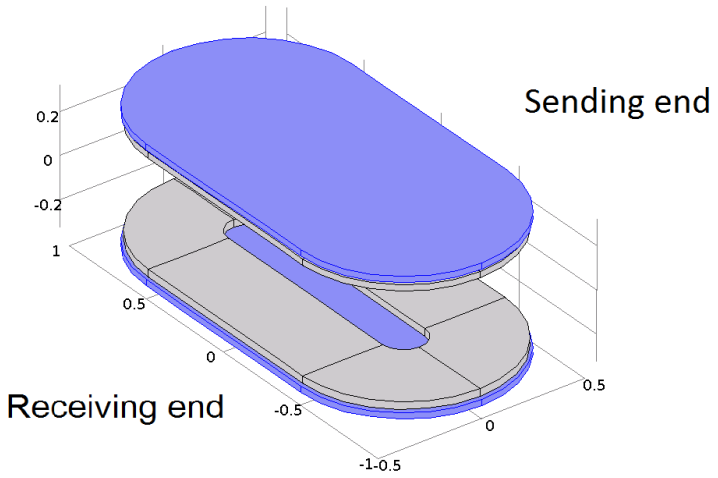

Figure 3.4 - Full scale 3D model of the IPT system

3.2. Considerations when making FEM models

One always has to be careful when using FEM software such as COMSOL Multiphysics and taking in to account that there are several possibilities for errors when making simulations. If everything is done correctly COMSOL should provide quite accurate results, but comparisons against physical measurements on identical coils should be done when possible.

4. Verification of method by measurements on a real coil

4.1. Creating a reference model

The basic for all simulations in this report are models built in COMSOL Multiphysics which is a complex simulation program, and the results must be interpreted with the proviso that there may be some errors. When a full scale prototype of the IPT system is ready, full scale measurements of the electromagnetic field must be done and the field strength must be evaluated by NRPA before it can be applied for any use in public. At this point, only a small scale prototype is built, but it has a resonance frequency above 100 kHz which makes it difficult to measure EMC field with the instruments available at this time. Therefore, in order to achieve greater credibility to the measurement results, a new model based on an inductor that is found in the local storage at SINTEF energy is built in COMSOL. The coil and the 3D model are shown in Figure 4.1.

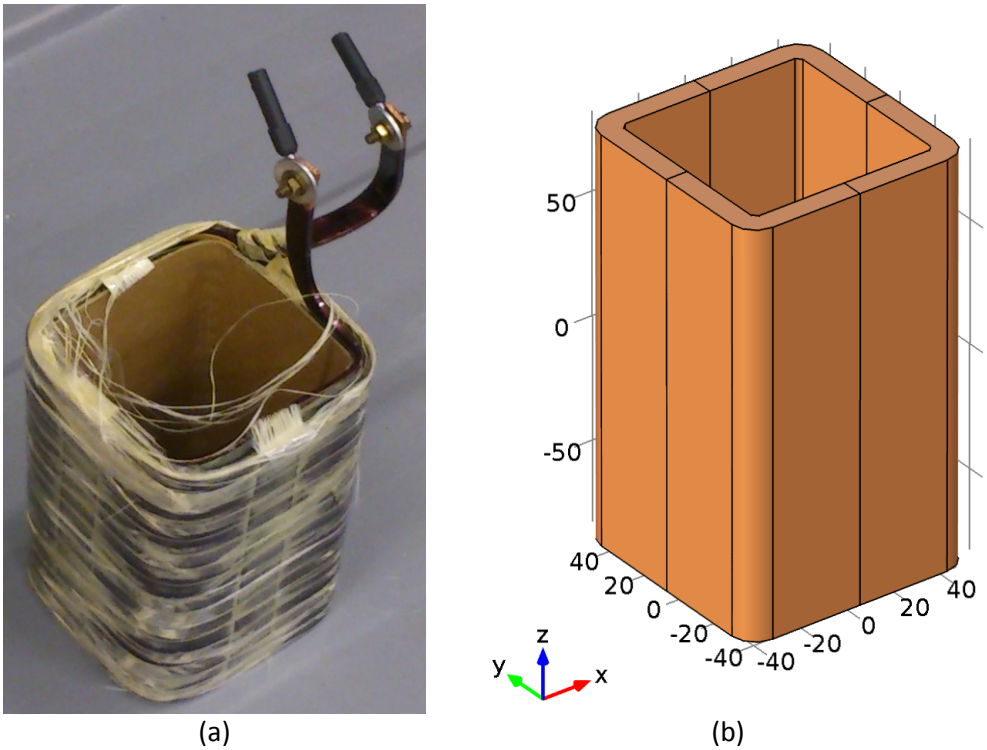

(a) (b)

Figure 4.1 - A representative coil is found at SINTEF storage (a), and then a 3D model of this coil is built in COMSOL Multiphysics (b). The purpose is to verify that the 3D models are built correctly and that COMSOL is reliable as tool for computing electromagnetic fields.

The coil is then tested in COMSOL with an applied current of 10 A, 50 Hz frequency which is plotted in Figure 4.2.

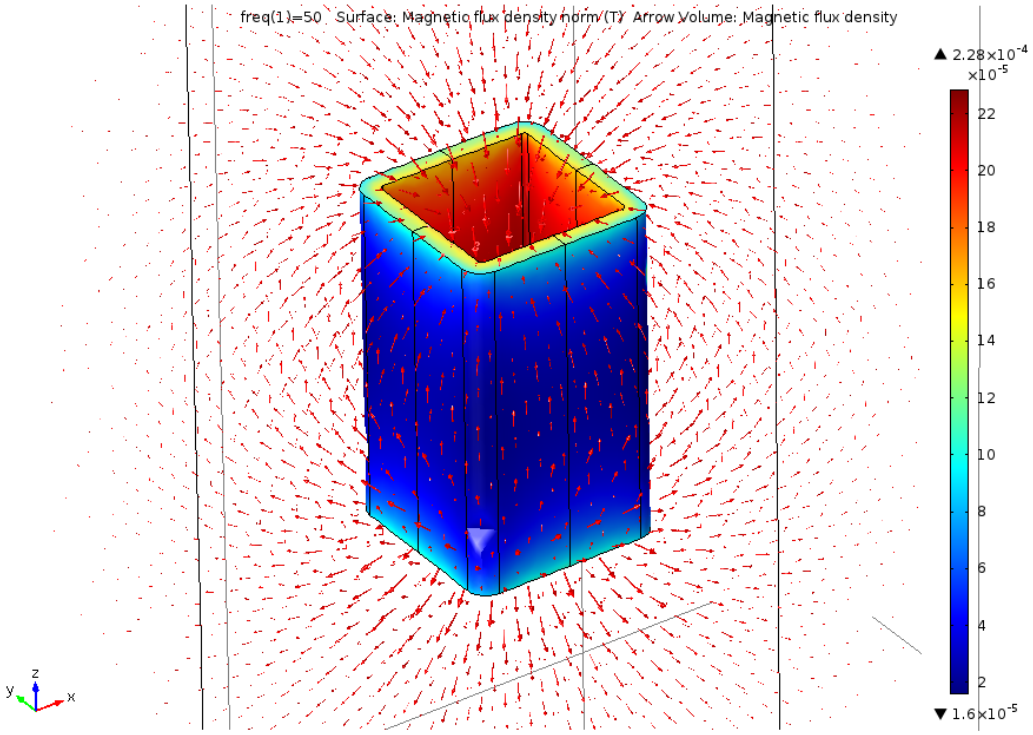

Figure 4.2 - Surface plot of magnetic flux density in addition to arrow plot indicating magnetic flux.

The flux density is the measured at specified distances from the bottom of the coil.

Test coil properties:

Outer dimension: 95 x 95 x 165 mm
Thickness: 9 mm
Conductor dimension: 3.3 x 11 mm
Number of turns: 2 x 16

The coil found at SINTEF does not come with any given properties. They are therefore calculated based on measurements of the coil. Inductance *L* is computed as:

$$L = \frac{2 \cdot W}{i_{RMS}^2} \tag{5.1}$$

where *W* is the energy evaluated by COMSOL and i_{RMS} is applied current. For the case with 10 A applied current, the total electric energy of the coil is integrated in COMSOL to be 2.11e-5 J which leads to an inductance of 0.42 µH.

The resistance, *R* is computed as:

$$R = \frac{\rho \cdot l}{A}$$

$$l = 95 \cdot 4 \cdot 32 \; [mm]$$

$$A = 3.3 \cdot 11 \; [mm] \tag{5.2}$$

where ρ is the conductivity for Cu which is 1.68e-2 (Ω·m) and *A* is the coil conductor cross-section area.

4.2. Physical tests of reference model

The computations performed in COMSOL must now be verified by connecting the actual coil to a 10 A current source. The applied voltage, *U* is computed as:

$$U = I \cdot (R + jX_L)$$

$$X_L = 2\pi f L \tag{5.3}$$

Substituting eq. 5.1 and 5.2 in to 5.3 gives the voltage:

$$U = I \cdot \left(\frac{\rho \cdot l}{A} + \mathrm{j}2\pi f \cdot \frac{2 \cdot W}{i_{RMS}^2} \right) \tag{5.4}$$

which results in an applied voltage of 5.8 mV. It will therefore be necessary to use a 220/12V transformer in addition to a variac that is connected to a 230 V outlet, as shown in Figure 4.3.

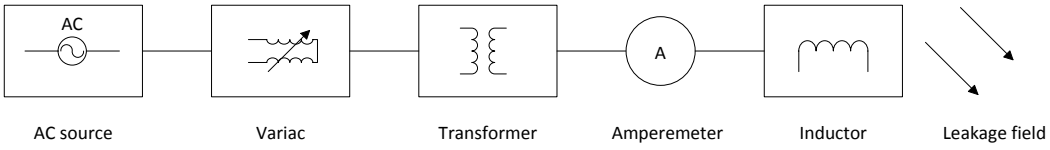

Figure 4.3 - Single line connection diagram for coil radiation test set-up.

Measuring instruments

For the magnetic field measurements done in this experiment, two instruments are used; Narda EFA-300 [16] and a Magnetic field meter, BM2 with lab number N1-004. Both instruments work by the same principal according to Faradays law of induction that a time-varying magnetic field within an enclosed loop will create an electric field that can be measured. Simply put, it means that the instruments have three coils oriented in respectively in z, y, and z direction, shown in Figure 4.4. Each of the coils measures the magnetic field on one axis and then the instrument sum up all three axes to a total magnetic field strength. A photo of the probes is shown in Figure 4.5, and all equipment used for this test is listed in Table 4.1.

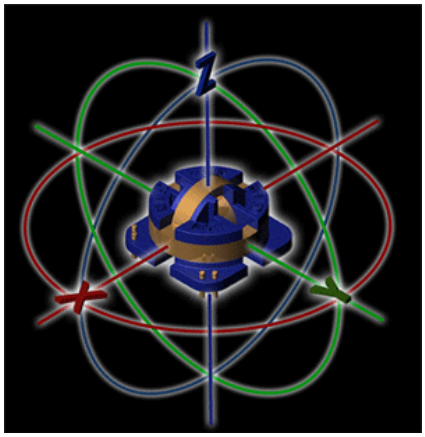

Figure 4.4 - Principle of EMC field analyzer [17].

Figure 4.5 - Analog EMC field analyzer probe and Narda EMF-300 probe.

Table 4.1 - List of equipment used for EMC field analyzis.

Equipment	Manufacturer / Type	Number
Coil		9. SINTEF storage
Variac	Lübcke	BI-0568
230/12 Transformer	Eltrafo AS	BI-0203
Amperemeter	Fluke / 336	I04-0487
Analog field analyzer	Radians Innova AB/ Magnetic field meter BM-2	N01-0004
Digital field analyzer	Narda/ EFA-300	N01-0017

With the coil energized, the magnetic field strength is measured with both analog instrument and Narda at certain distances from the coil which is pictured in Figure 4.6.

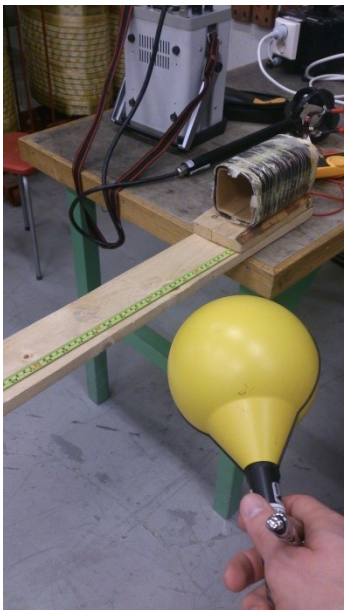

Figure 4.6 - Photo of test set-up.

The results from the experiment with the two respective instruments in addition to results from COMSOL simulations are presented in Table 4.2

Table 4.2 - Magnetic flux density at a given distance from the bottom of the coil measured with two different EMC analyzers in addition to computations made in COMSOL.

Magnetic flux density [µT]										
Distance [cm] / **Instrument**	30	40	50	60	70	80	90	100	150	200
BM2 EMC instrument	**65.0**	**20.0**	**9.0**	**4.0**	**2.0**	**1.40**	**1.0**	**0.62**	**0.18**	**0.06**
Narda EMC instrument	**30.0**	**16.0**	**7.20**	**3.70**	**2.20**	**1.37**	**0.93**	**0.68**	**0.22**	**0.12**
COMSOL	**35.71**	**12.55**	**5.30**	**2.72**	**1.56**	**0.88**	**0.60**	**0.40**	**0.06**	**0.01**

To better compare the results they are plotted in a graph showing flux density as function of distance from the bottom end of the coil shown in Figure 4.7.

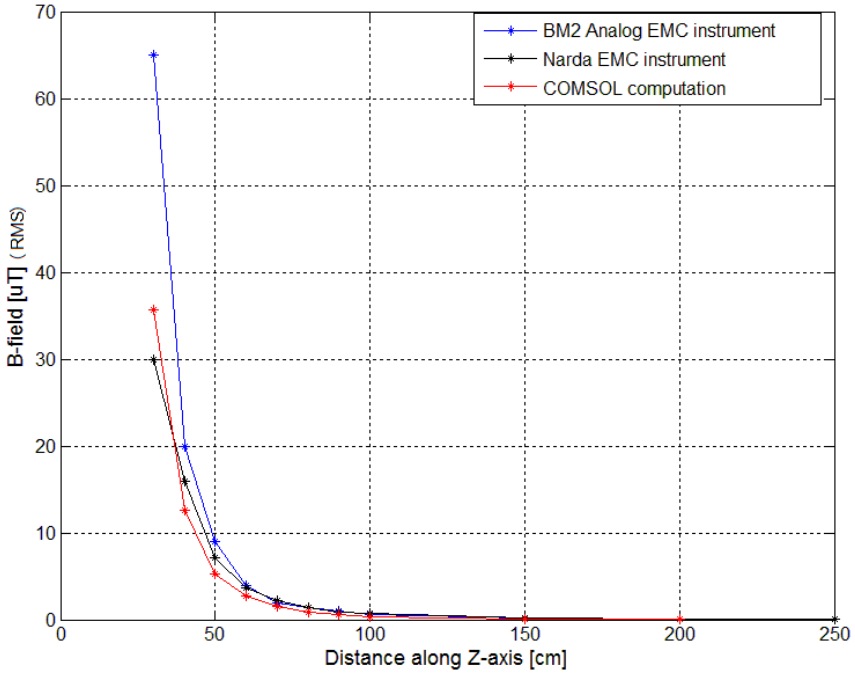

Figure 4.7 - Graph showing EMC field strength for the two EMC analyzers and the computations done in COMSOL Multiphysics.

The results from the field measurements indicates that all values on magnetic field strength lay in the same range, but that there is a significant deviation between the Narda instrument and the analog instrument, which can mainly be explained in two ways: The Narda was recently calibrated before this test [18], while there is no documentation on when the analog instrument was calibrated. Also, it could be that the analog instrument displays peak value instead of RMS, but the documentation on the BM-2 does not provide information about this.

Also the size of the probe will be of importance for the accuracy in the field near the coil, since the field varies a lot just by a few millimeters. The probe measuring the field seems to be a little larger for the analog instrument which can be seen from Figure 4.5. At the distance of two meters the field strength produced by the coil is so weak that noise from other electrical devices in the room will be dominating. Even with the coil not energized the field strength in this area did not go below 0.1 µT.

The test is now done again, but this time with a copper plate in front in a distance of about 30 cm from the bottom end of the coil to test the effect of shielding as shown in Figure 4.8.

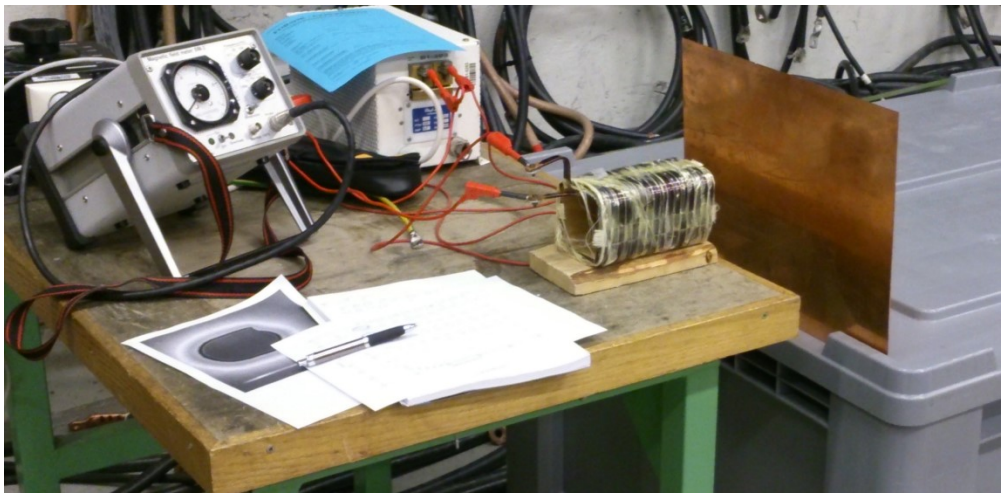

Figure 4.8 - Photo of test set-up with a copper plate in front of the coil to test the effect of electromagnetic shielding.

The electromagnetic field strength is then measured again with the just the Narda field analyzer at time because it is assumed to be more reliable than the analog BM-2 field analyzer. Also the field strength at 30 cm could not be measured in this case because the probe would come in conflict with the copper plate. Test results are presented in Table 4.3.

Table 4.3 - Magnetic flux density at a given distance from the bottom of the coil measured with the Narda EMC field analyzer and compared to computations made in COMSOL.

Magnetic flux density [µT]									
Distance [cm] / **Instrument**	30	40	50	60	70	80	90	100	150
Narda EMC instrument	**N/A**	**9.0**	**4.5**	**2.5**	**1.3**	**0.9**	**0.65**	**0.45**	**0.13**
COMSOL	**27.60**	**7.85**	**3.53**	**2.29**	**1.20**	**0.74**	**0.49**	**0.32**	**0.05**

Test results indicate a small deviation of approximately 10%. The test numbers are also shown graphically in Figure 4.9.

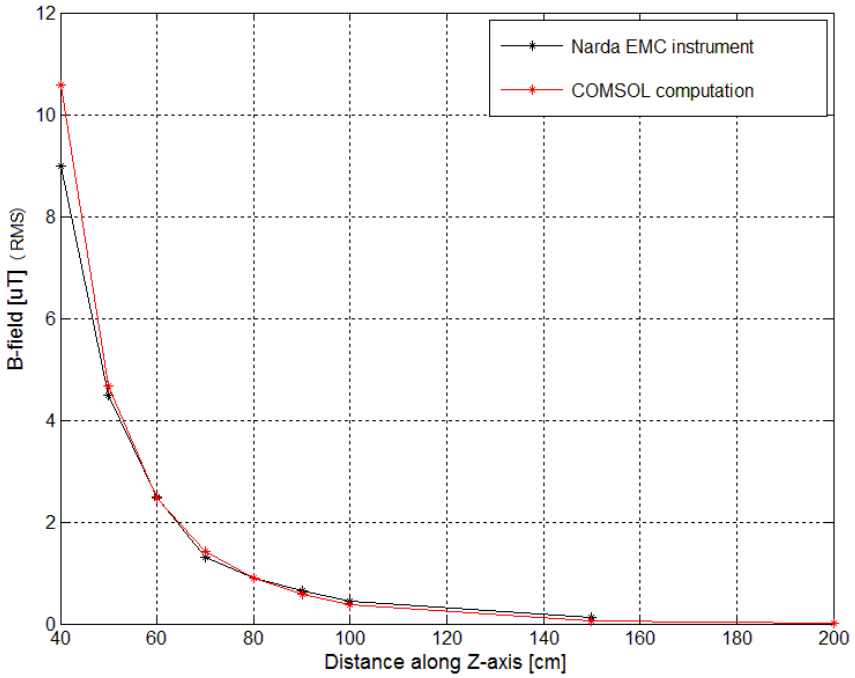

Figure 4.9 - Graph showing EMC field strength measured by the Narda EMC field analyzer and the computations done in COMSOL Multiphysics.

4.3. Summary of simulations with the reference model

The lab test described in this chapter has been an attempt to evaluate the reliability of using FEM software to analyze electromagnetic fields by comparing 3D simulations of a coil to the actual coil. The results between COMSOL and physical measurement seem to be very close with the largest deviation in the region closest to the coil.

5. Shielding

5.1. Shield testing in COMSOL

In order to investigate the effects of shielding with various configurations, new models of the IPT system with additional geometry that will be specified as aluminum is created. To shorten computation time, some models are made in 2D axisymmetric modelling to get a picture of the effects of shielding, and then some models are tested out in full 3D. Only full size 3D models are made for these tests because models drawn using symmetry lines will not be able to test the effect of misalignment.

Various shielding configurations will be applied to the model and considered regarding efficiency, losses in the material and loss of efficiency in the power transfer. The configuration of the coil remains the same and is given in Table 5.1.

Table 5.1 – Specifications from SINTEF report [1] of IPT design evaluated in COMSOL

Design parameters	
Cores	
IPT Width, w_b	1.0 m
IPT Length, l_b	2.0 m
Backplate thickness, h_b	2.81 cm
Windings	
N1, N2	8, 8
Winding width, w_w	0.389 m
Winding height, h_w	3.37 cm
Gaps	
Backplate/winding clearance, W_{ins}	1 cm
Converter parameters	
Operating frequency	3.37 kHz
Maximum current	1430 A_{RMS}

The power transferred by the IPT will vary depending on the coupling coefficient, *k* described briefly in [1], but the current in the two coils might have phase shift up to 90 degrees.

5.2. Effect high permeability material

Permeability, μ is the ability of a material in a magnetic field to form a magnetic field, in other words the degree of magnetization that a material obtains when it is exposed to a magnetic field. The permeability constant, μ_0 also known as the magnetic constant is described as the permeability in vacuum and is $4\pi \cdot 10^{-7}$ (H/m). A *diamagnetic* material has a permeability, μ_d lower than μ_0 and a *paramagnetic* material has a permeability, μ_p higher than μ_0. Refer to Figure 5.1 for illustration of relationship between *B*, *H* and μ. *Ferromagnetic* materials have a very high permeability, μ_f and will therefore work as good magnetic conductors. Ferrite is a ferromagnetic material and may therefore be applied to obtain better control of the electromagnetic field that occurs around the IPT system.

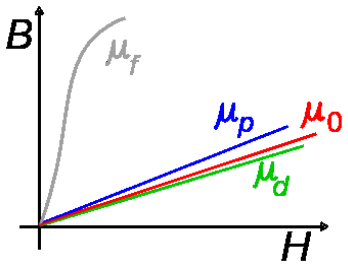

Figure 5.1 - B-H curve [19].

A simulation of the 2D model described in section 3.1.1 is now performed with the configurations given in Table 5.1 with current through receiving end coil lagging by a 90° phase shift. A plot with phase angle at 0° without ferrite backplate is shown in Figure 5.2 (a) and a plot with ferrite backplate is shown in Figure 5.2 (b). Figure 5.2 (c) and Figure 5.2 (c) shows the same plots, but at a 45° phase angle. In the plots the cross-section (z-x axes) area of the coils and the ferrite core can be seen, and they are intended to illustrate how much of the field that goes in the ferrite and how much that is leaked to the surroundings.

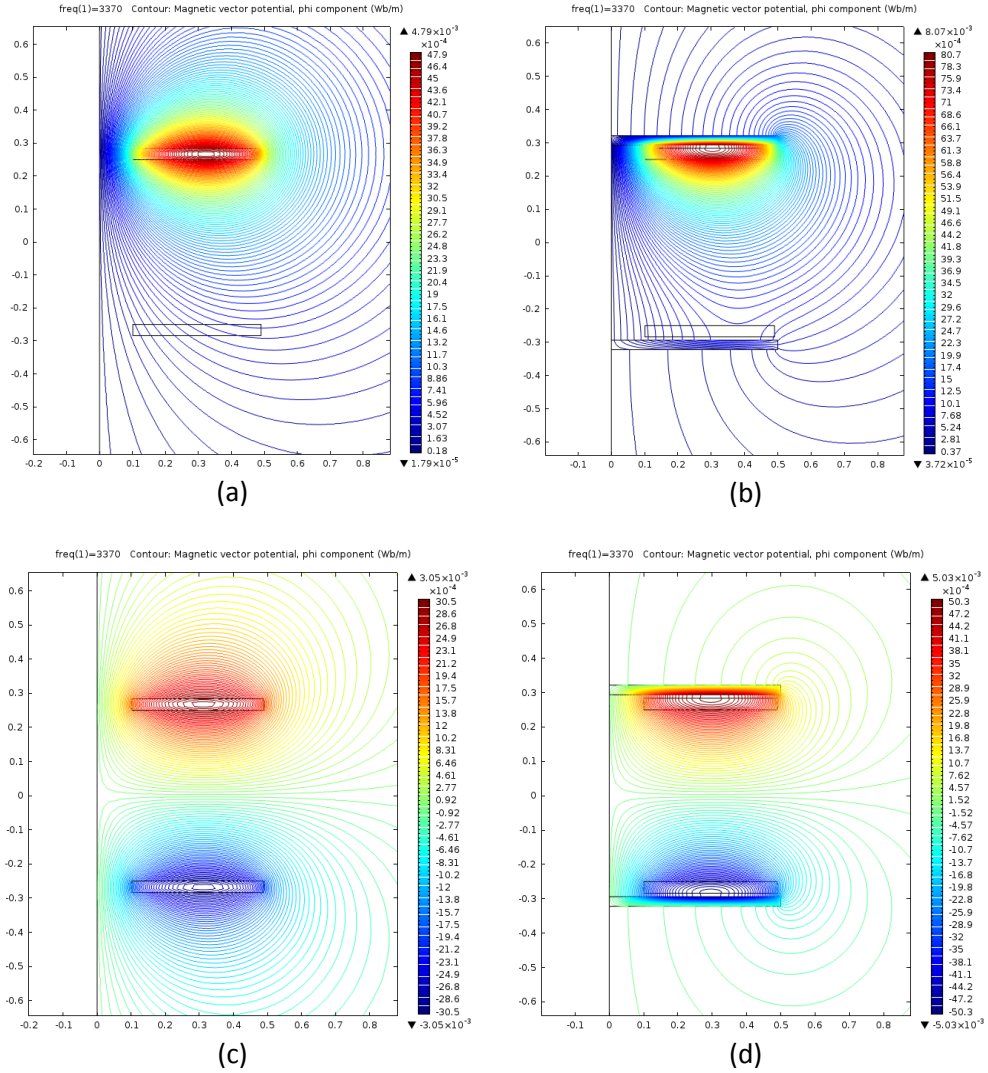

Figure 5.2 - Plot of magnetic field strength between sending and receiving end where;

(a) – No ferrite backplate with phase at 0°.

(b) – Ferrite backplate with phase at 0°.

(c) – No ferrite backplate with phase at 45°.

(d) – Ferrite backplate with phase at 45°.

Distance is given in meters.

Figure 5.3 (a) and (b) shows a plot of the magnetic flux density without and with the ferrite core focused in the area between 0 to 0.01 T. The plots indicate that the ferrite reduces the field strength significantly at the outside of the IPT, but increases it between the coils. Lower magnetic field leaked to the surroundings will help decreasing losses in conducting materials in the near field region.

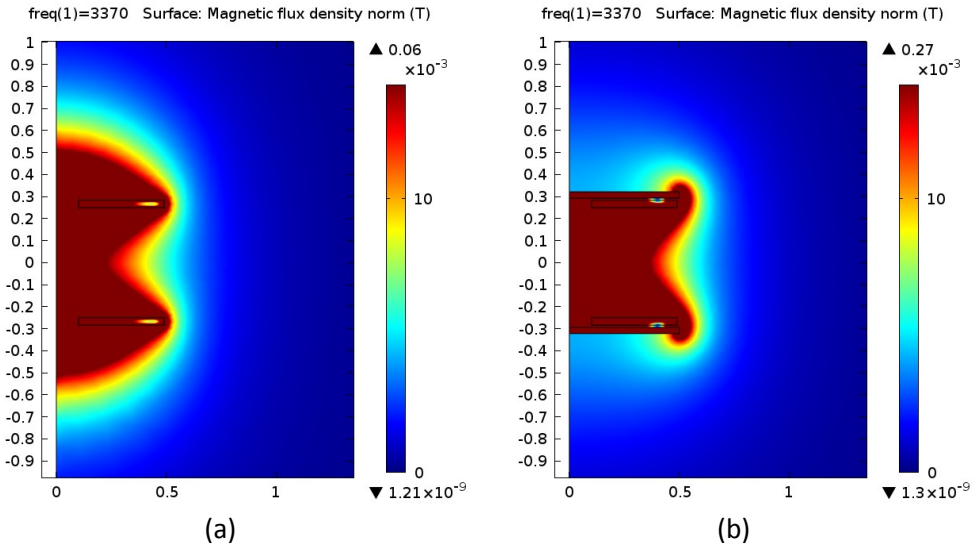

Figure 5.3 - Plot of magnetic flux density norm done in a 2D axisymmetric model focused in the range from 0 - 0.01 T where (a) is with no ferrite backplate and (b) is with ferrite backplate. Distance is given in meters.

As the highest recommended flux density for general public was specified to be 6.25 µT in the ICNIRP guidelines from 1997 and adjusted to 27 µT in 2010, the field strength in the plot shown in Figure 5.4 is focused in the range from 6 – 30 µT to investigate if the ferrite makes any difference in this region.

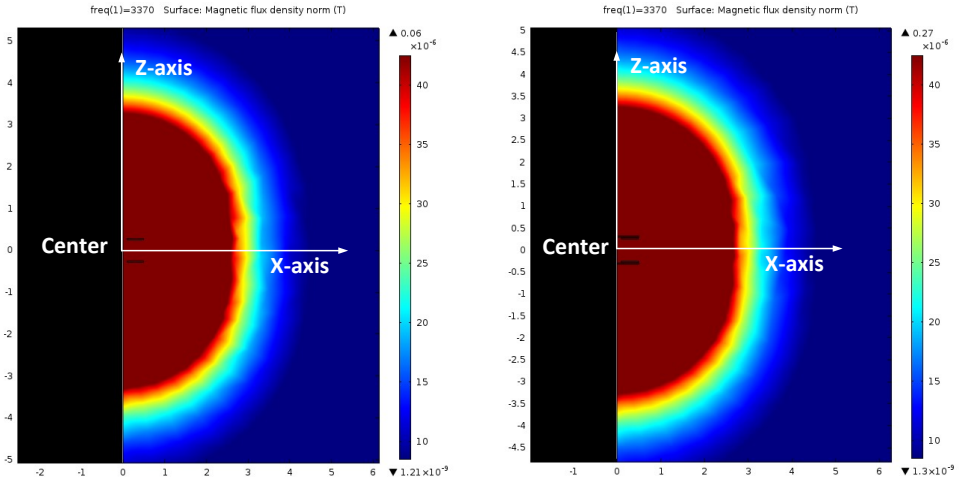

(a) (b)

Figure 5.4 - Plot of magnetic flux density done in a 2D axisymmetric model focused in the range from 6 - 30 µT where (a) is with no ferrite backplate and (b) is with ferrite backplate.

The plots in Figure 5.4 show that the ferrite backplate has almost no effect to the flux density in the weaker field region. To show numerically how the magnetic field spreads, the flux density along the axes specified in Figure 5.4 is plotted as a function of distance from the center.

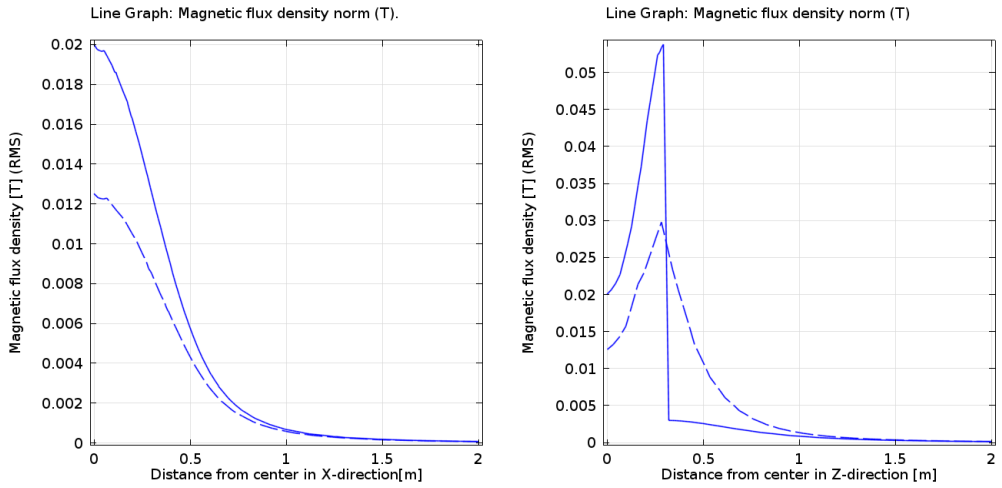

(a) (b)

Figure 5.5- Plot of magnetic flux density where (a) is the field strength from center between the coils along X-direction, and (b) is from the centre and out in z-direction. Solid line = with ferrite. Dashed line = without ferrite.

The numerical graphs of the flux density confirms that the ferrite backplate only has effect in the near field region, but already from 1 meter and outwards, the effect is minimal.

5.3. Shielding using a high conductive material

Ferrite is very beneficial to use as a core backplate since it will direct the magnetic field in a specified direction and therefore increase the efficiency of the inductive power transfer. However there is still a leakage field that surrounds the coils and the shielding effect of the ferrite is, as mentioned above, not that significant in the area with lower magnetic field density. This means that there still has to be a considerable safety distance which will require space. In order to reduce the field strength and by that the space occupied for safety distance, some additional shielding must be added.

If a material with high electric conductivity such as copper or aluminum is exposed to a time-varying magnetic field, there will be induced an electric field in the material as given by Faradays law of induction (eq. 6.1). Lenz law [20] says that the electric field will be opposite but proportional to the rate of change in the magnetic field, and therefore the electric field will induce currents that sets up a magnetic field in the opposite direction of the applied field as illustrated in Figure 5.6.

$$\varepsilon = -\frac{\partial \Phi_B}{\partial t} \tag{6.1}$$

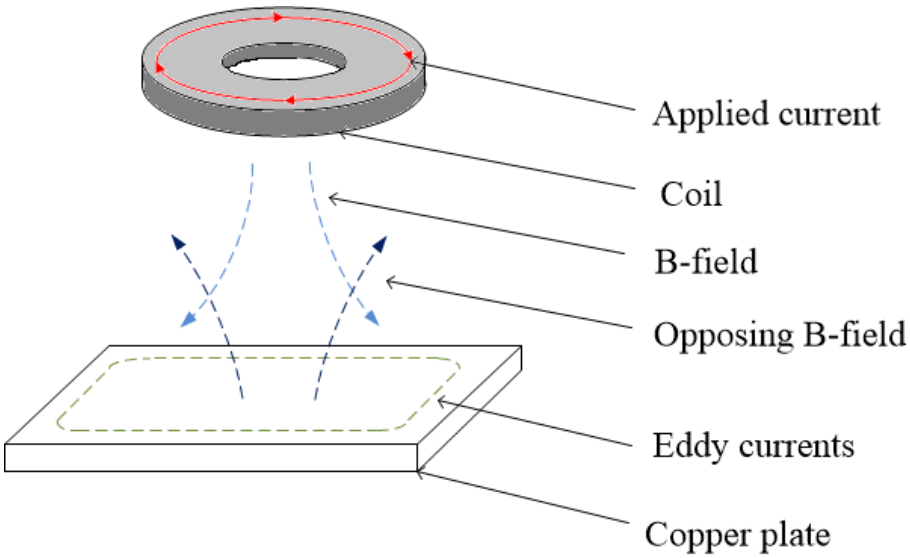

Figure 5.6 – When a copper plate is exposed to a time-varying magnetic field, it will set up a field with equal flux density in the opposite direction and thus the area behind the plate will be shielded from the field.

The effect of shielding depends on the electrical resistance of the copper plate, which again depends on the penetration depth, also called *skin depth* of the induced currents. Skin depth, δ as given in eq. 3.2 depends on the materials electrical conductivity σ, permeability $\mu_0\mu_r$ and the applied frequency, f:

$$\delta = \frac{1}{\sqrt{\pi\mu_0\mu_r\sigma f}} \tag{3.2}$$

Since the copper is not a perfect electric conductor, the current produced by the electric field will not be able to set up a magnetic field with the same magnitude as the applied field, however better conductivity of the copper plate cause lower resistance and thus higher current. Conclusively, increasing the thickness of the plate will increase the efficiency of the shielding.

If for example a magnetic field of 50 Hz is applied on to the copper plate, 63% the induced eddy-currents would penetrate 9.2 mm into the material, but the depth is logarithmically decreasing so that if the plate was 15 mm thick the resistance for the induced current would be so low that it would set up an opposing magnetic field with almost the same magnitude as the applied field.

5.4. 2D modelling of shielding

This section will expand the 2D models of the IPT with ferrite backplate and add various configurations of shielding consisting of aluminum. Plots of flux density are still focused in the range from 6 – 30 μT. As these are 2D plots the distances where the field reaches are not entirely correct, but still they should print a good image on how the field responds to shielding.

The IPT system considered in this study is meant to be fitted on ships, primarily ferries which suggest that it will probably be placed on a ship side consisting of aluminum. An aluminum plate is added to the 2D model and the size of the plate is an assumption based upon the new battery driven ferry that will be put in traffic between Larvik and Oppedal from 2015. According to Siemens [21] the ferry will consume 200 kWh per trip, thus if this ferry would be charged with a 1 MW power transfer by the IPT it would take 12 minutes to charge the ferry, neglecting losses.

The area of aluminum plate supposed to be the ship side is set to 5 x 10 meters (but just modelled as 5 meters for the 2D modelling) assuming that there are no other obstacles on this side.

Specifications of the IPT are otherwise the same as given in Table 5.1, but in addition there is added an aluminum shielding specified in Table 5.2. The geometry is shown in Figure 5.7.

Table 5.2 - Shielding configurations

Shielding	
Screen dimension	5 x 10 m
Screen thickness, h_{Al}	2.0 cm ([2])
Ferrite Backplate/screen clearance, g_s	10 cm

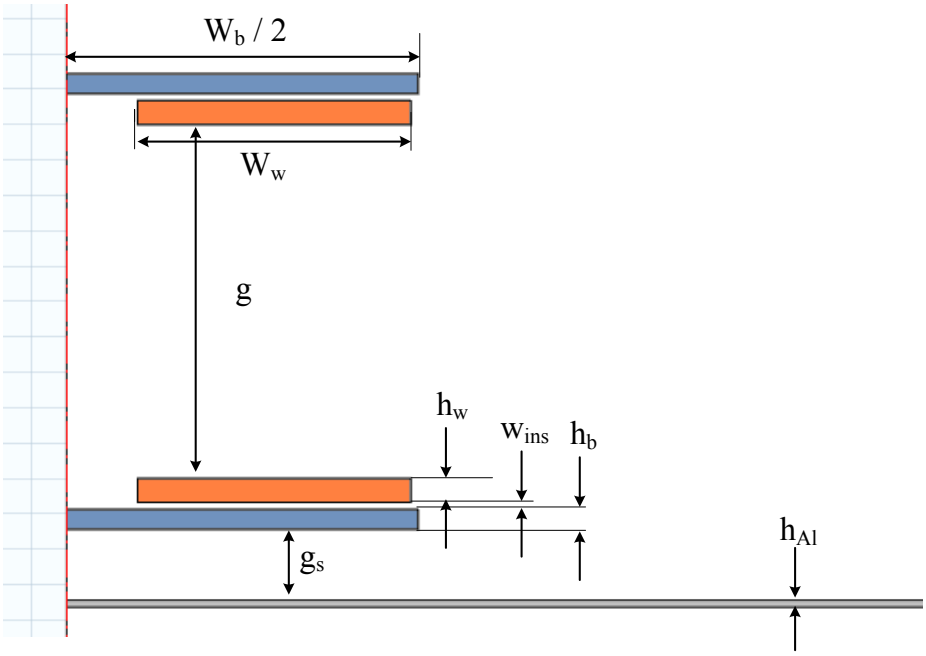

Figure 5.7 - IPT geometry specifications with terms elaborated in table 5.1 and 5.2.

[2] Skin depth for aluminum at 3.37 kHz is 1.5 mm according to eq. 3.2.

5.4.1. Aluminum ship side

A geometry specified as aluminum is now added to the same model described in section 5.2. The result is then plotted and shown in Figure 5.8 with focus on the field range from 6 - 30 µT, same as in Figure 5.4.

The index "*mf.normB/sqrt(2) (T)*" means that the plot and scale is the magnetic flux density normal which is the sum of all vectors given in RMS values. COMSOL will always assume amplitude values[3] so therefore currents used in the simulations are always specified as $(I * sqrt(2))$.

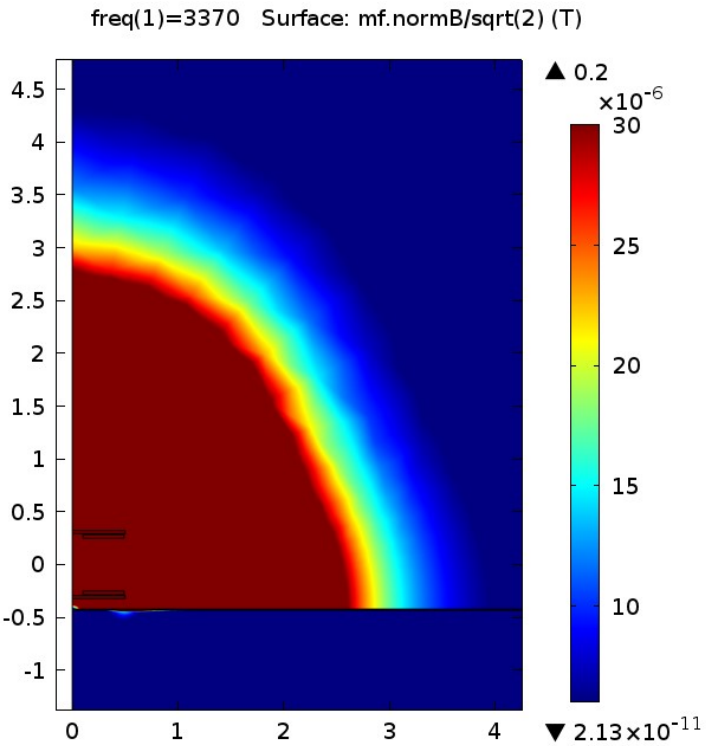

Figure 5.8 - Plot of magnetic flux density focused in the range from 6 – 30 µT with just ship side.

The plot indicates that the aluminum will prevent the magnetic field radiation above recommended values from penetrating in to the ship. Further, it reduces the distance for the same flux density by approximately 0.5 meter.

Details on how the field responds to shielding can be seen in Figure 5.9.

[3] Confirmed by e-mail correspondence with COMSOL support.

(a)

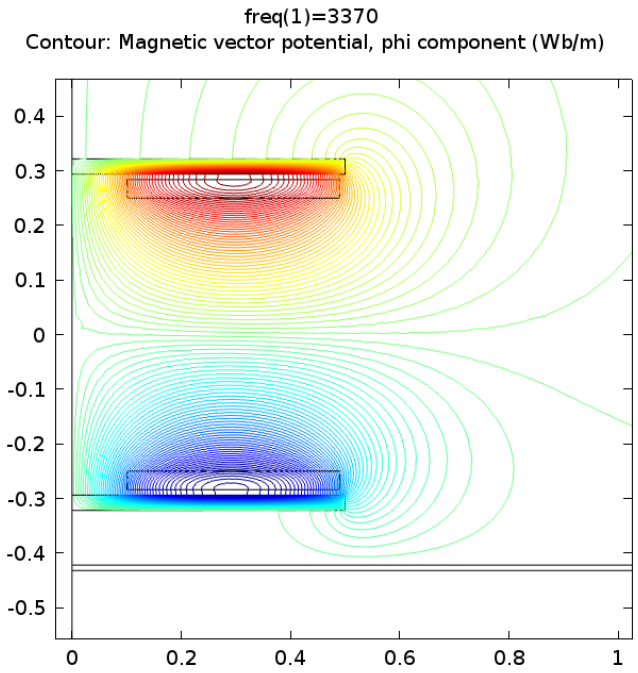

(b)

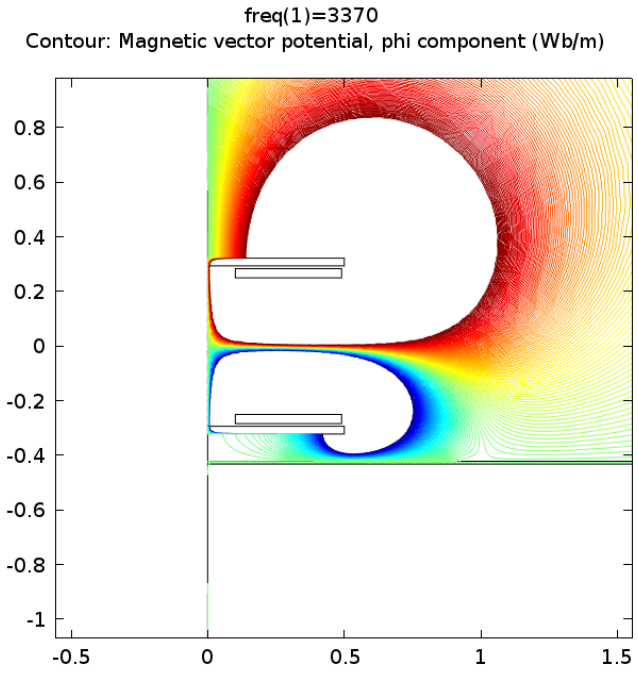

Figure 5.9 - Plot of magnetic field strength between sending and receiving end with ship side present. Plot (a) is in range between ±5 mT and (b) is ±100 µT.

5.4.2. Shielding added to receiving end

I addition to the aluminum plate, a vertical screen can be added that surrounds the coils. The height of this screen is the same as the sum of the gaps, backplate and coil so that the clearance to the opposite end still is 0.5 meters. The distance from the backplate to this vertical screen is 20 cm. However, the plot of magnetic flux density, shown in Figure 5.10 indicates that this shielding has little extra effect.

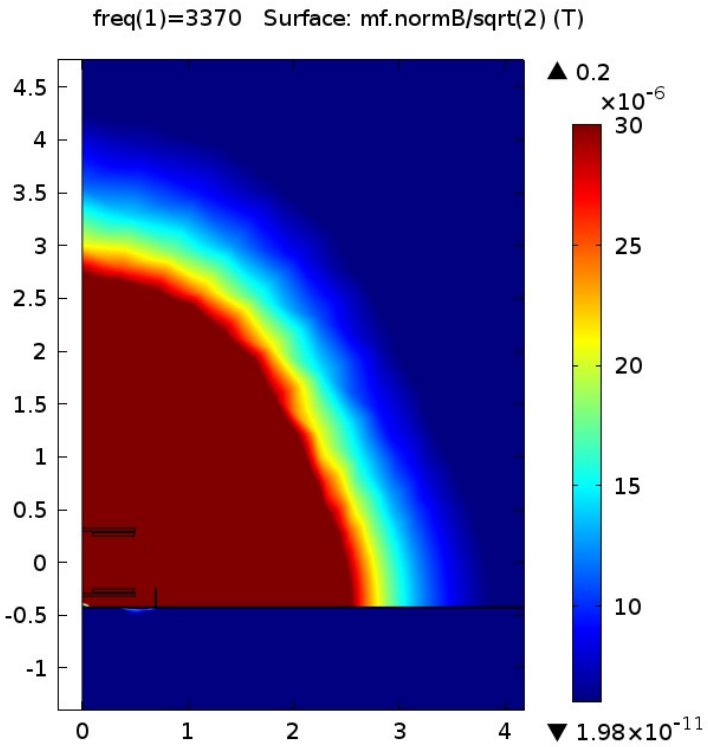

Figure 5.10 – Plot of magnetic flux density focused in the range from 6 – 30 µT with screen put on ship side.

By comparing the plots from Figure 5.9 with the plots in Figure 5.11, it shows clearly why the extra shielding on receiving end has little effect.

(a)

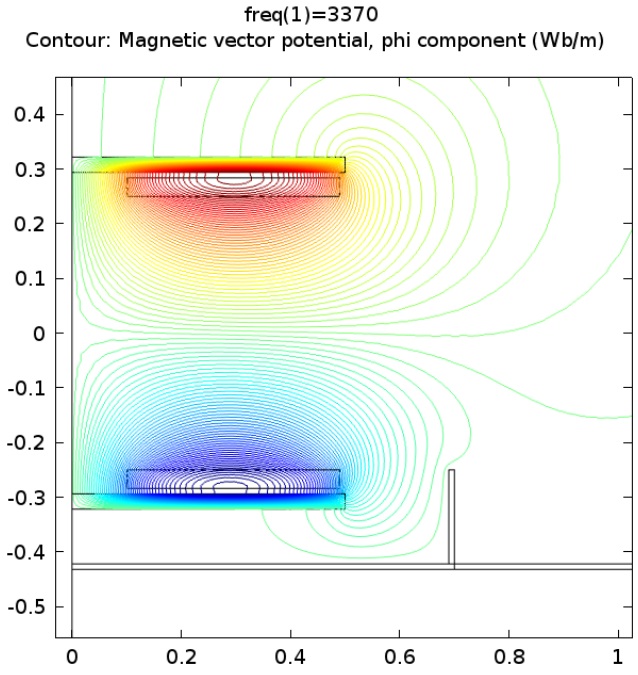

(b)

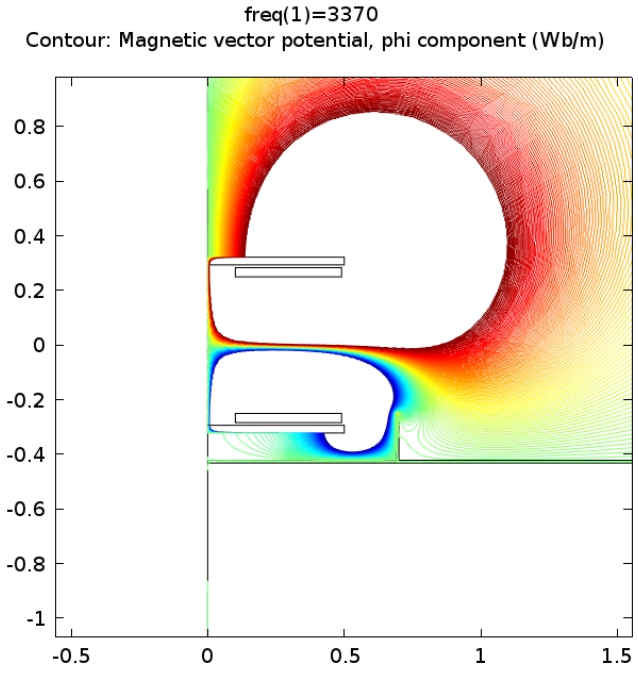

Figure 5.11 - Plot of magnetic field strength between sending and receiving end with ship side and lower shielding present. Plot (a) is in range between ±5 mT and (b) is in range between ±100 µT.

5.4.3. IPT recessed in ship hull

Another possible and very interesting solution is to have the receiving end recessed in to the ship side instead of mounting it on to the side. In addition to better shielding, it will also provide more mechanical protection of the receiving end, but it will still keep the same mechanical clearance to the sending end. As the plot in Figure 5.12 shows it has a certain effect on the field.

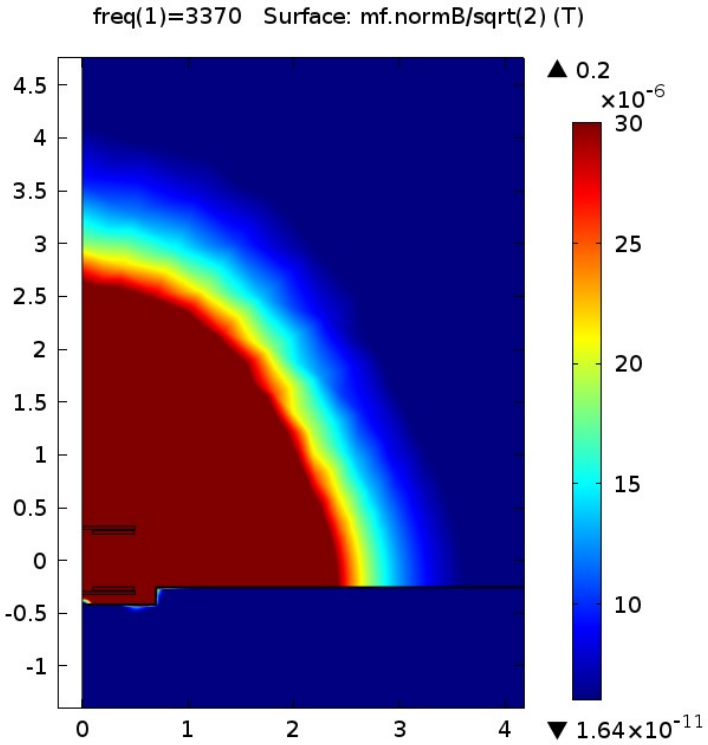

Figure 5.12 – Plot of magnetic flux density focused in the range from 6 – 30 µT with IPT system recessed in ship.

The plot of the vector potential shown in Figure 5.13 shows that the magnetic field from the sending end now is the dominating in to the surroundings.

(a)

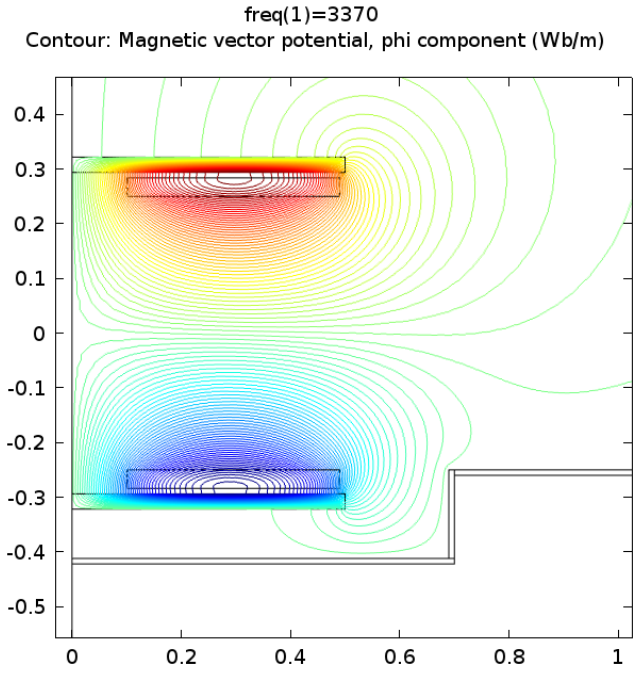

(b)

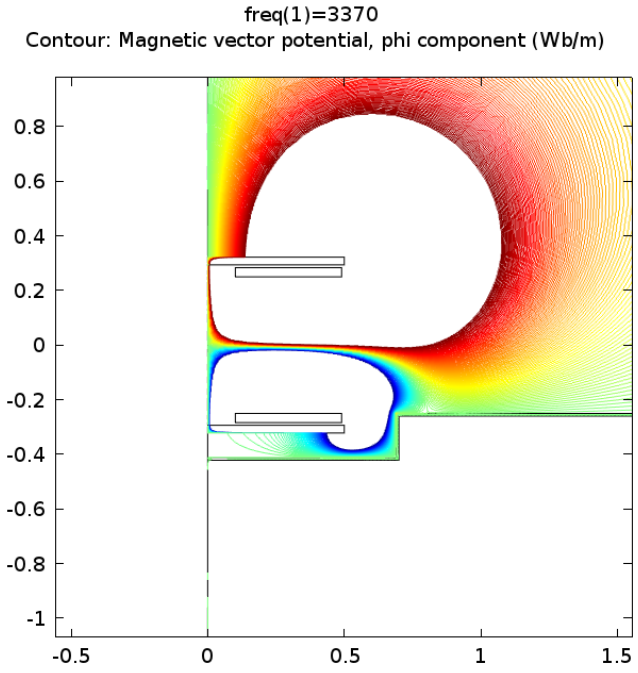

Figure 5.13 - Plot of magnetic field strength between sending and receiving end with receiving end recessed in ship side. Plot (a) is in range between ±5 mT and (b) is ±100 µT.

5.4.4. Aluminum shielding applied to sending end.

If shielding is added to the sending end, it should reduce the field leaked to the surroundings significantly. For this case, shielding only on sending end is applied in addition the ship side which clearly has an effect as can be seen plotted in Figure 5.14.

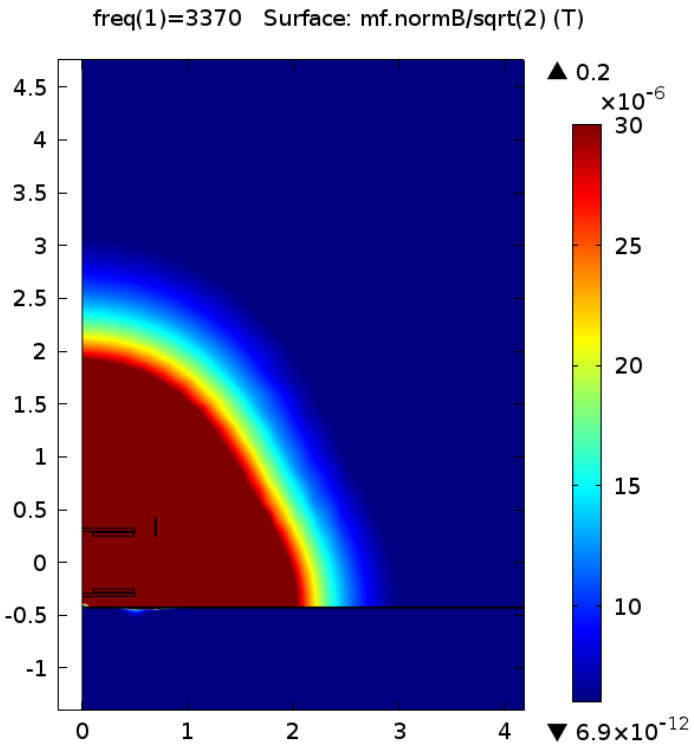

Figure 5.14 – Plot of magnetic flux density focused in the range from 6 – 30 µT with shielding added to sending end.

A plot of the vector potential is shown in Figure 5.15, and out of this plot it seems that the upper shielding has the most effect in addition to the aluminum plate.

(a)

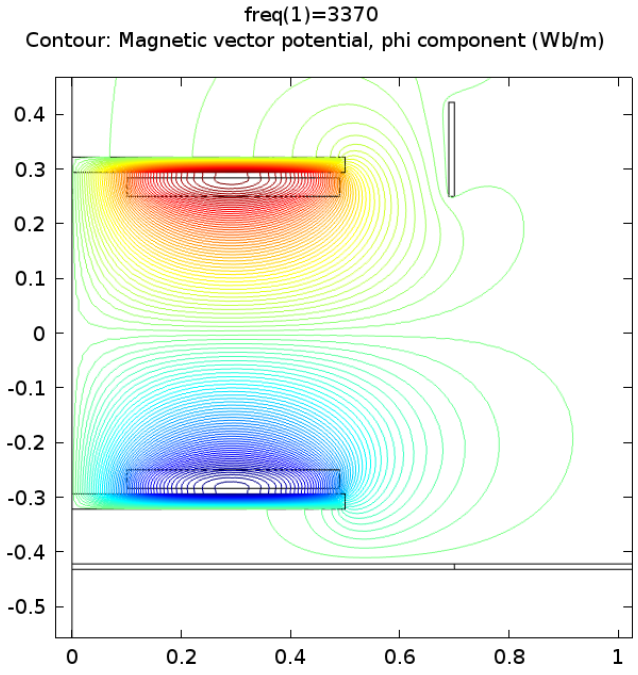

(b)

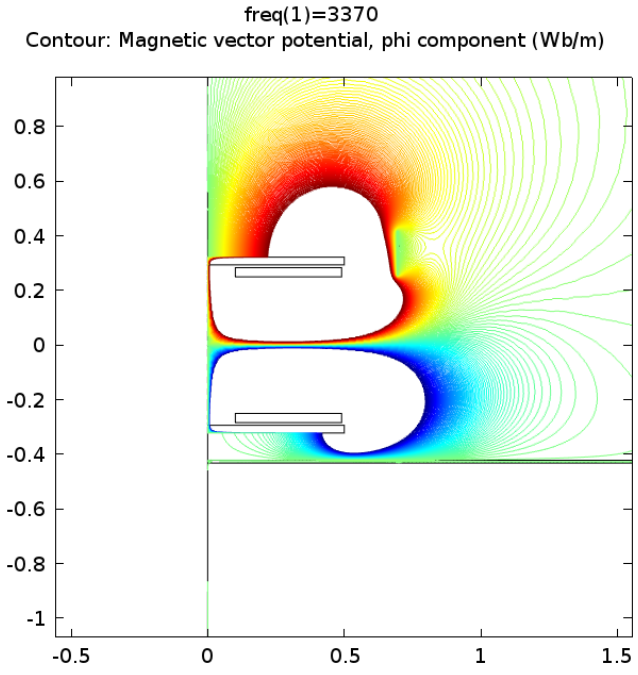

Figure 5.15 - Plot of magnetic field strength between sending and receiving end with screen applied to sending end. Plot (a) is in range between ±5 mT and (b) is ±100 µT.

5.4.5. Shielding added to sending and receiving end

In addition to shielding on sending end, shielding is now applied to receiving end as well. The extra shielding on receiving end has, as expected little effect to the total field which can be seen on the plot in Figure 5.16

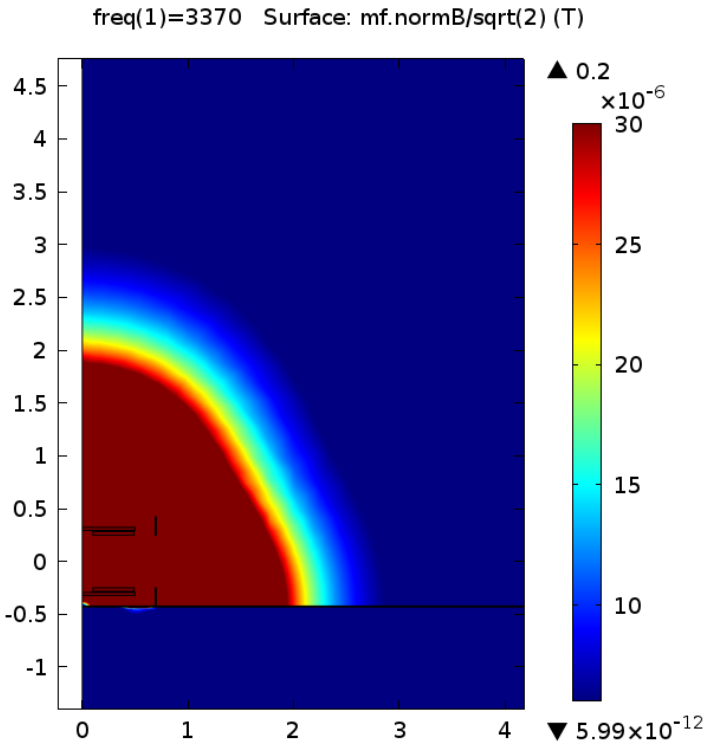

Figure 5.16 - Plot of magnetic flux density focused in the range from 6 – 30 µT with shielding added to sending and receiving end.

The magnetic vector potential is plotted in Figure 5.17 which shows why the additional lower shielding does not have much effect in addition to aluminum plate.

(a)

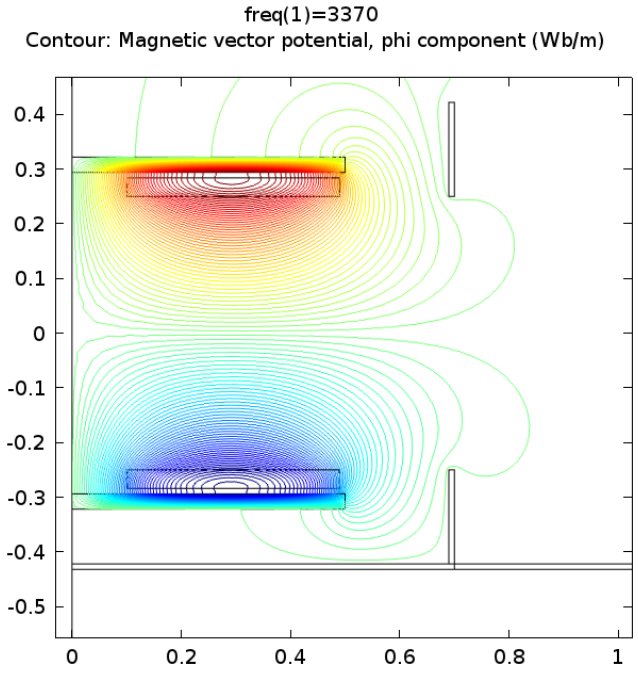

(b)

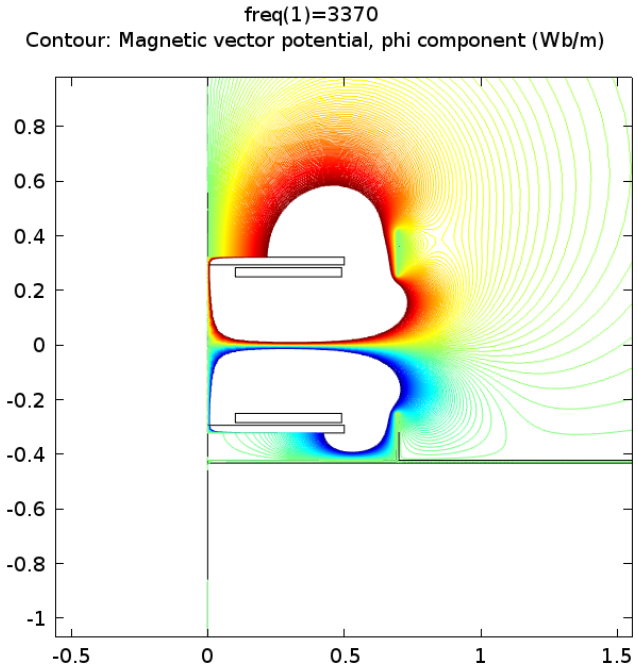

Figure 5.17 - Plot of magnetic field strength between sending and receiving end with shielding applied to both sending and receiving end. Plot (a) is in range between ±5 mT and (b) is ±100 µT.

5.4.6. IPT recessed in ship hull with aluminum shielding on sending end

With shielding applied to sending end, the receiving end is also recessed in ship side, which also reduces the distance of the leaked magnetic field by approximately 10 cm as shown in Figure 5.18.

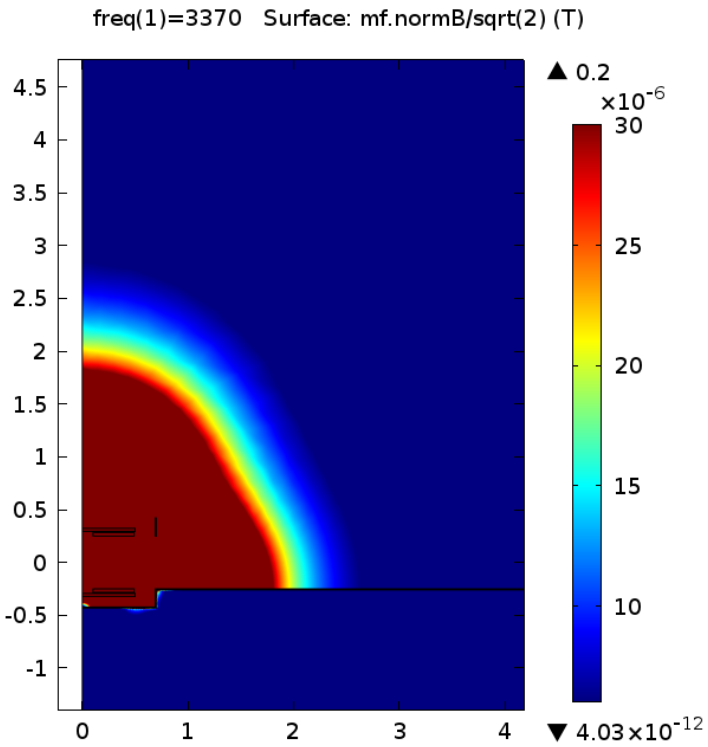

Figure 5.18 – Plot of magnetic flux density focused in the range from 6 – 30 µT with receiving end recessed in ship side with upper shielding added.

The effect of the shielding can be examined more detailed from the plots in Figure 5.19.

(a)

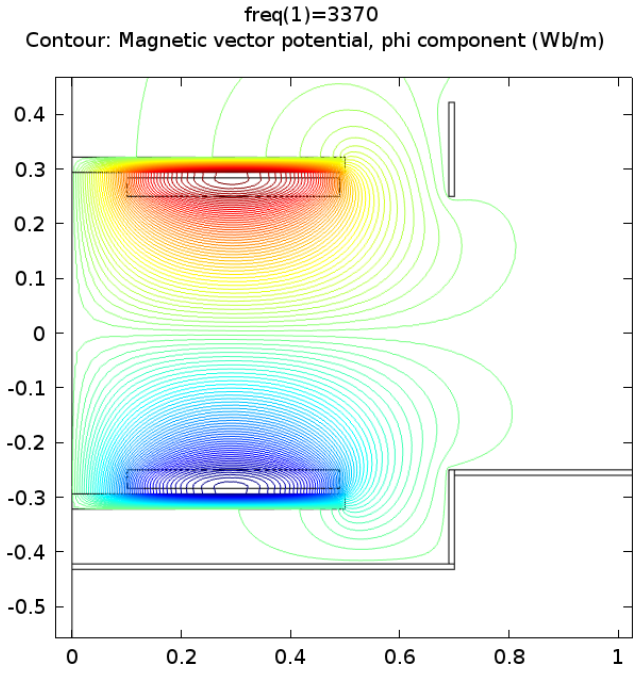

(b)

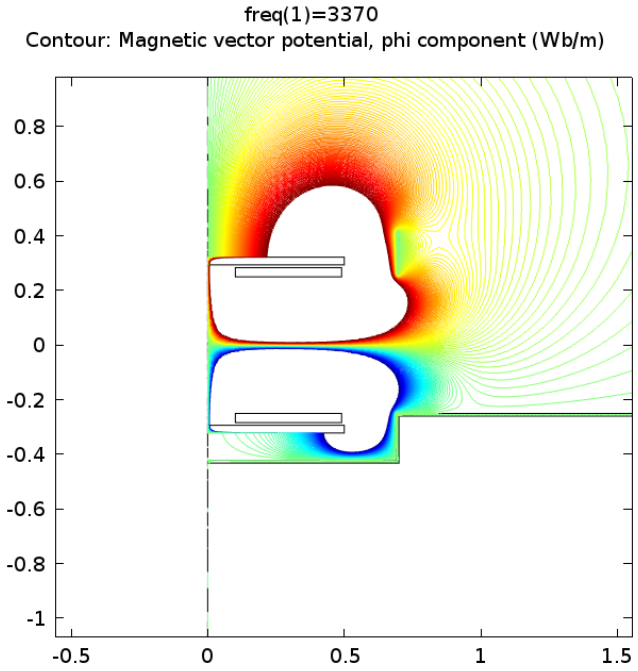

Figure 5.19 - Plot of magnetic field strength between sending and receiving end with receiving end recessed in ship side and shielding applied to sending end. Plot (a) is in range between ±5 mT and (b) is ±100 µT.

5.4.7. Shielding on rear side of sending end

Aluminum backplate is now added to sending end in order to reduce the field leaked in Z-direction, that is the direction outwards of the ship. This will create an enclosed shielding around the sending in all directions that is not towards the receiving end and has a significant effect to the leakage field, as shown in Figure 5.20.

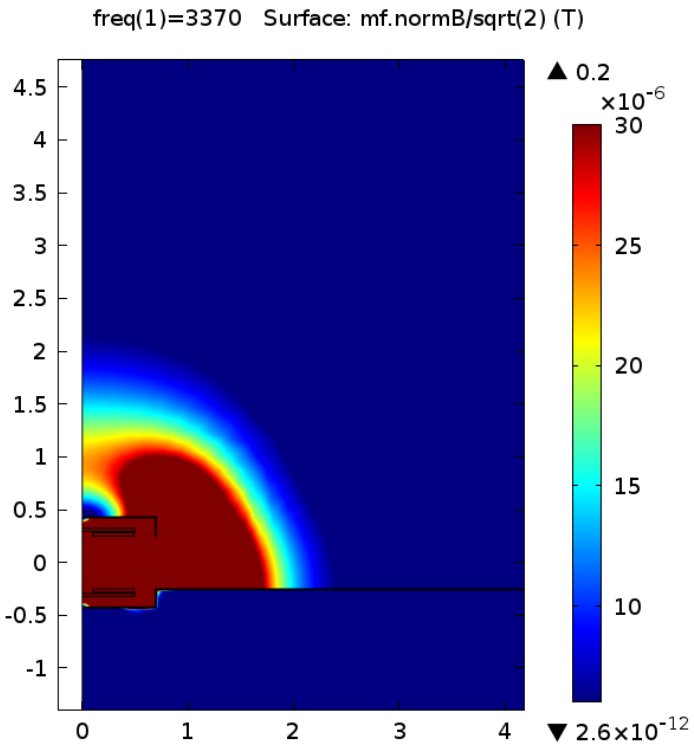

Figure 5.20 – Plot of magnetic flux density focused in the range from 6 – 30 µT with receiving end recessed in ship side with upper enclosed shielding added.

Details of the magnetic field can be seen from the plot in Figure 5.21.

(a)

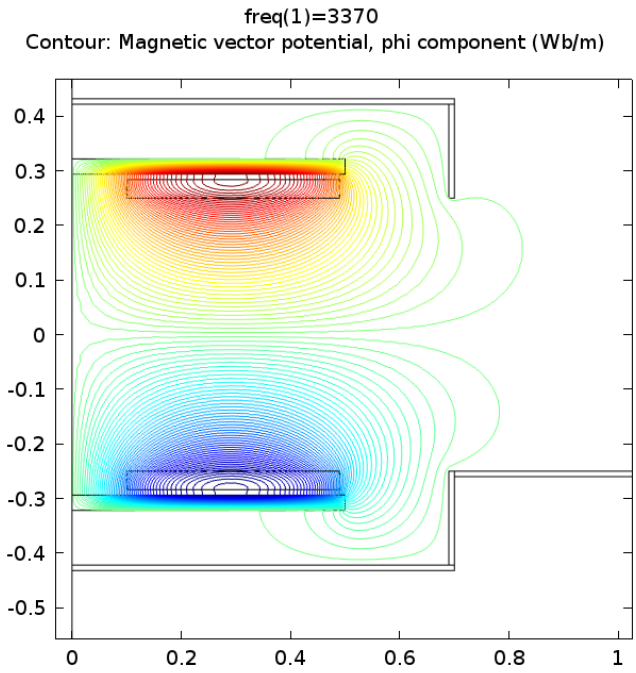

(b)

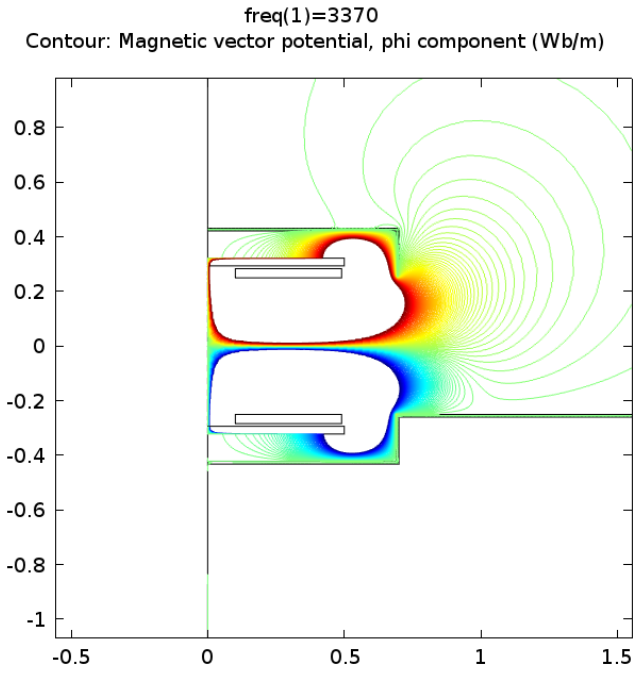

Figure 5.21 - Plot of magnetic field strength between sending and receiving end with receiving end recessed in ship side and enclosed shielding applied to sending end. Plot (a) is in range between ±5 mT and (b) is ±100 µT.

5.4.8. Extended shielding on sending end

To minimize the magnetic field as much as possible, the shielding on the sending end could be extended, similar to the shielding on receiving end.

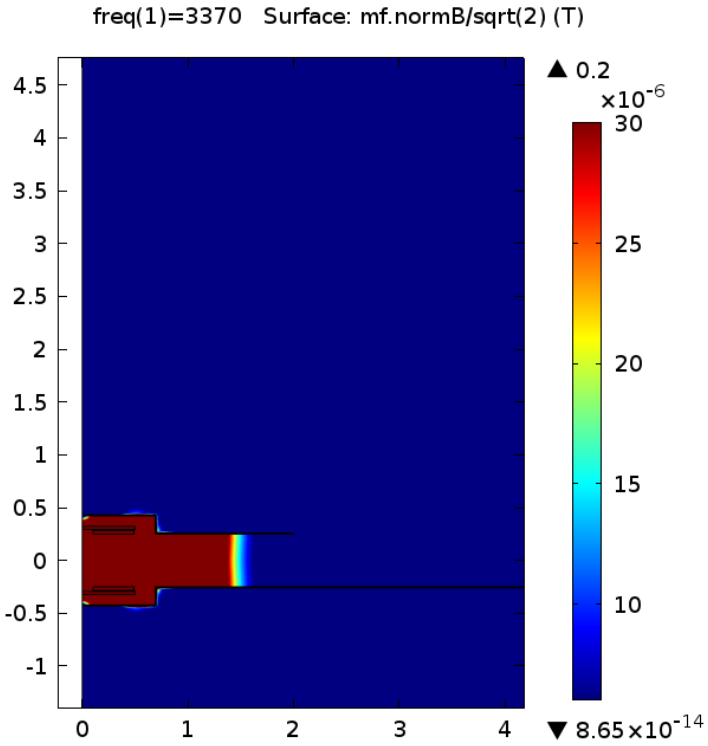

Figure 5.22 - Plot of magnetic flux density focused in the range from 6 – 30 µT with receiving end recessed in ship side and upper shielding enclosed and extended.

The field from the sending and receiving ends are now equally dominant which can be seen from the plots in Figure 5.23.

(a)

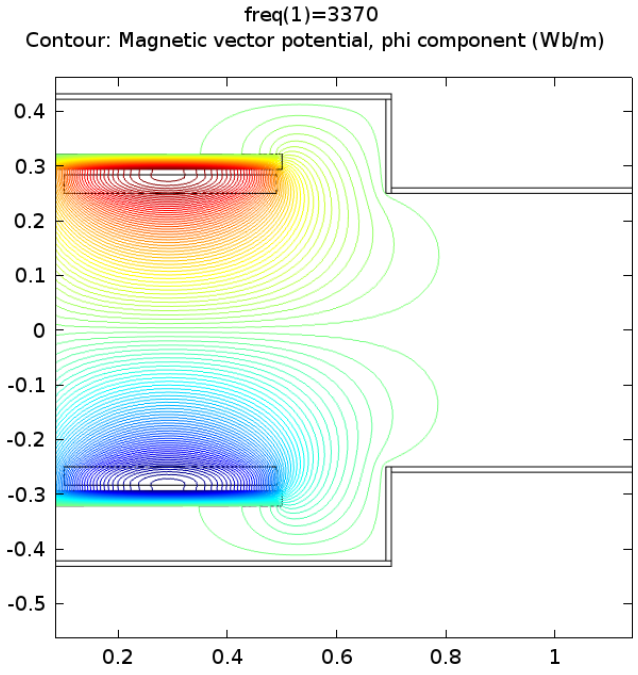

(b)

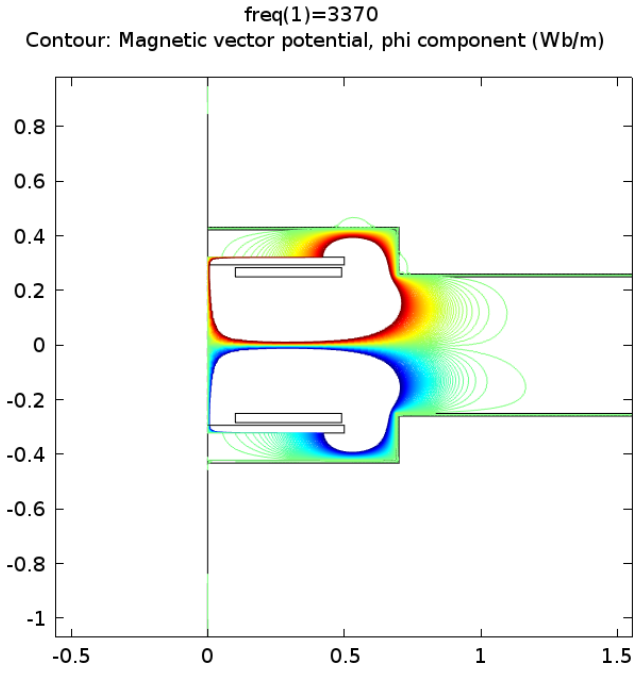

Figure 5.23 - Plot of magnetic field strength between sending and receiving end with receiving end recessed in ship side and enclosed extended shielding applied to sending end. Plot (a) is in range between ±5 mT and (b) is ±100 µT.

5.4.9. Summary of 2D simulations

This section has compared various configurations of shielding and shown which effect it has to the magnetic field produced by the IPT system. It has given a certain picture on how the field forms, but it has not given precise answers to how strong the magnetic field strength is because of the fact that a 2D simulation is only a simplification. Therefore, losses in the screen and numerical plots of the field strength have not been evaluated because the numbers would be inaccurate. In order to do more realistic evaluations on losses in screen and more precise values of the field strength, a full 3D analysis must be performed.

5.5. 3D modeling

To have more accurate analyses on the magnetic field produced by the IPT system, the modelling done in section 5.4 is now performed in 3D. The results from these simulations, which are with the same parameters as the 2D modeling, should come out similar but the fields will be larger. All tests in this section are done with the design parameters given Table 5.1 and Table 5.2, and the results will be analyzed considering flux density and effect of shielding. For better illustration, Figure 5.24 shows how the receiving end of the IPT system is mounted on a ship. Note the axes orientation and the coordinate system in this image, as the directions in all other plots will be referred to as X, Y and Z –axes;

- X-axis: Front/back of the ship
- Y-axis: Up/down of the ship
- Z-axis: Inward/outward of the ship

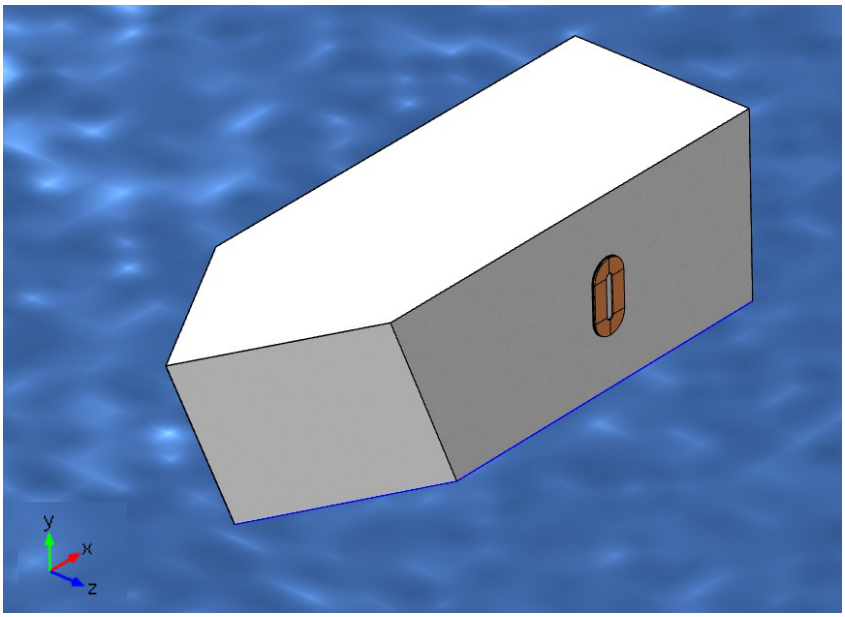

Figure 5.24 – Receiving end of IPT system mounted on ship.

5.5.1. No shielding

As a starting point, a 3D model of the IPT system with no shielding as shown in Figure 5.25 is considered to be compared with the 2D simulations.

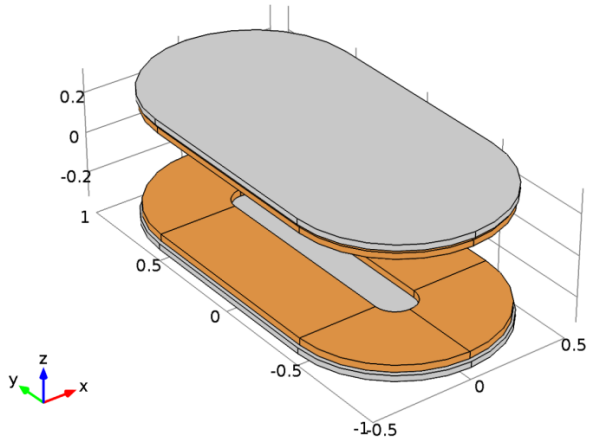

Figure 5.25 - IPT system with no shielding.

The magnetic flux density is now drawn in two 2D plots with Z-Y axes and Z-X axes respectively as shown in Figure 5.26. For comparing simulations in 3D with simulations in 2D, refer to Figure 5.4 (b).

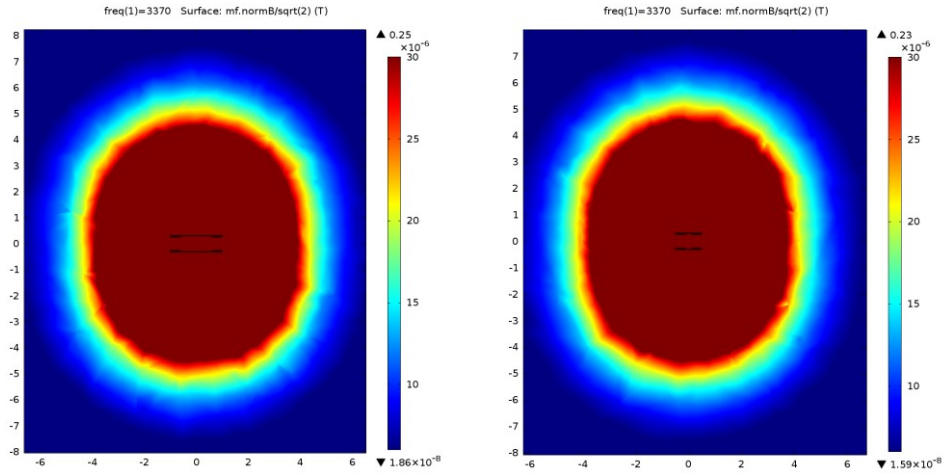

(a) (b)

Figure 5.26 – Plot of magnetic flux density focused in the range from 6 – 30 µT with no shielding applied. Figure (a) = Z-Y axes, figure (b) = X-Y axes.

As the results from the 3D simulation with no extra shielding shows, the magnetic field is stronger than 27 µT within four meters away from the center of the IPT.

5.5.2. Aluminum ship side

Because of the complexity of the model shown in Figure 5.24, it would it would be too resource-intensive to do the simulations on this model. The geometry is therefore simplified to just an aluminum plate with dimension 5 x 10 meters which is representing one side of the ship. This plate is now added to the 3D modelling in order to evaluate the field in both Y and X direction in addition to Z direction. Thought the shielding might have several options the ship side will most likely form some basic shielding depending on the design of the ferry.

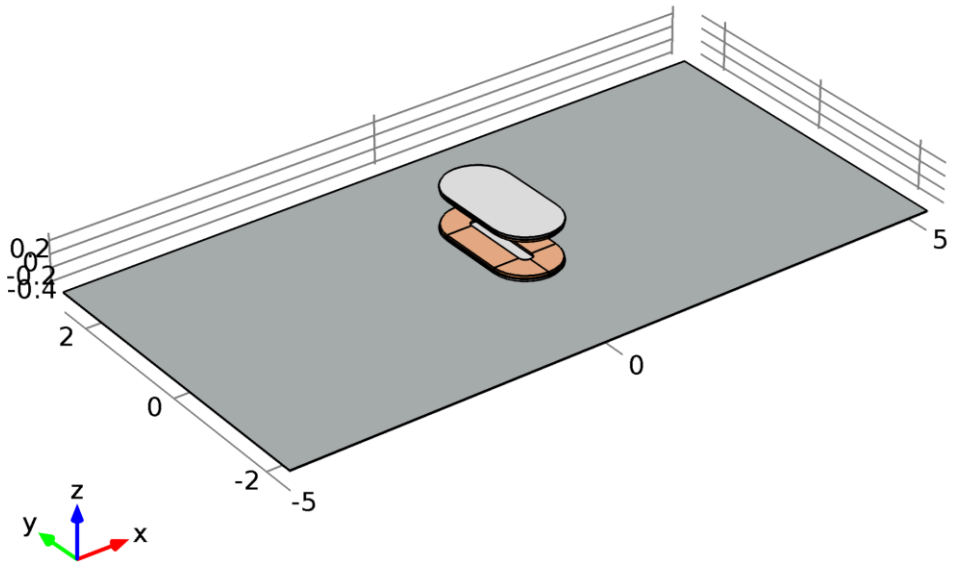

Figure 5.27 - IPT system with one side of the ship.

The magnetic field distribution can be seen in Figure 5.28 for Z-Y axes and Figure 5.29 for Z-X axes. There was also done a simulation with aluminum shielding without using the ferrite core backplate and the results shows, as expected that the losses in the shielding are significantly higher because of a stronger magnetic field.

Losses in aluminum plate: 391.47 W
Losses in aluminum plate without ferrite backplate: 3198.1 W

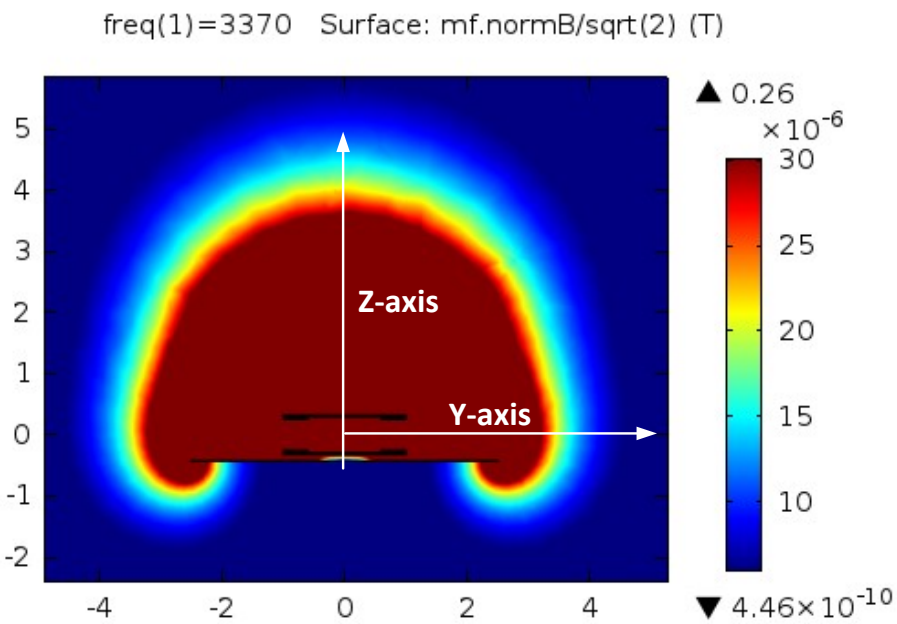

Figure 5.28 - Magnetic flux density plot focused in the range from 6 to 30 µT on Z-Y axes modelled with ship hull.

Magnetic field in vertical direction (Y-axis) appears to exceed the aluminum plate to some extent, but it is unlikely that there will be open space at bottom and the top of the ship. Also, the ship side does make any shielding to the field in outwards direction (Z-axis) from the IPT which means that with this configuration it will be necessary to keep clear distance for least three to four meters away from the sending end coil.

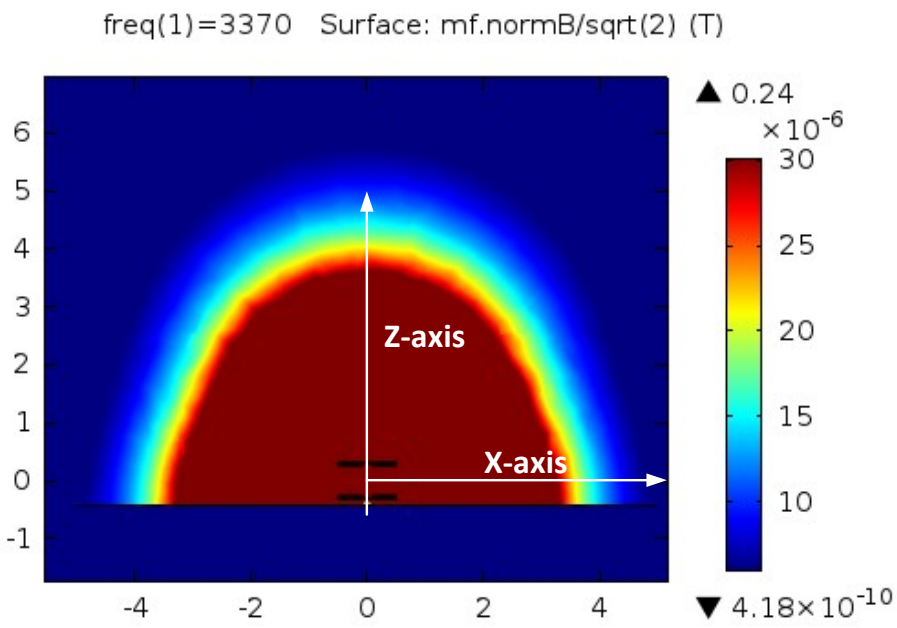

Figure 5.29 - Magnetic flux density plot focused in the range from 6 to 30 µT on Z-X axes modelled with ship hull.

The flux density along the line tagged Z-axis is plotted numerically in Figure 5.30 and the scale is logarithmical to compare the field before and after ship side shielding is added. This indicates that with the aluminum ship side the flux density just behind the plate is below 1 µT which is well below the highest exposure levels for general public recommended in the ICNIRP guidelines.

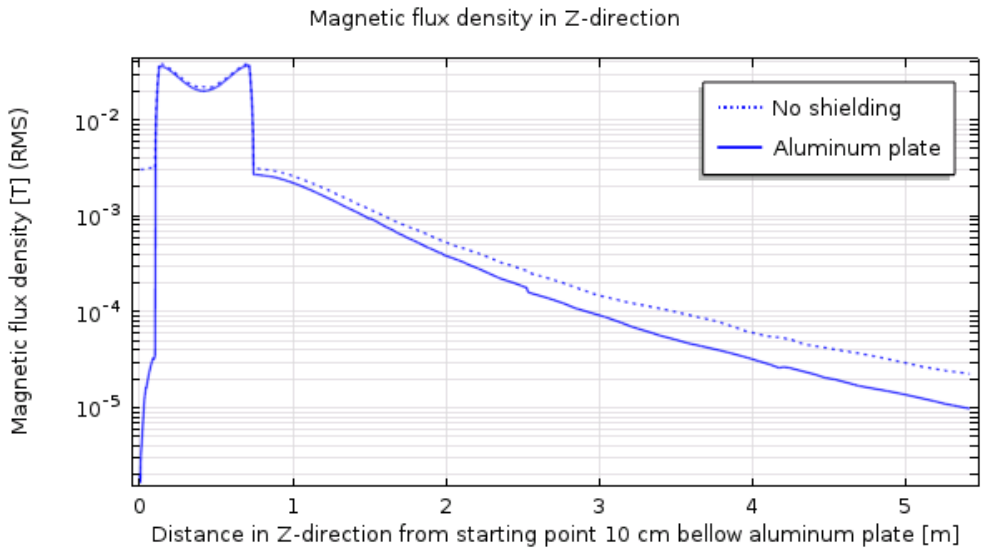

Figure 5.30 - Plot of magnetic flux density on Z-axis.

Magnetic flux density with and without aluminum plate is also evaluated in vertical direction of the ship, the Y-axis.

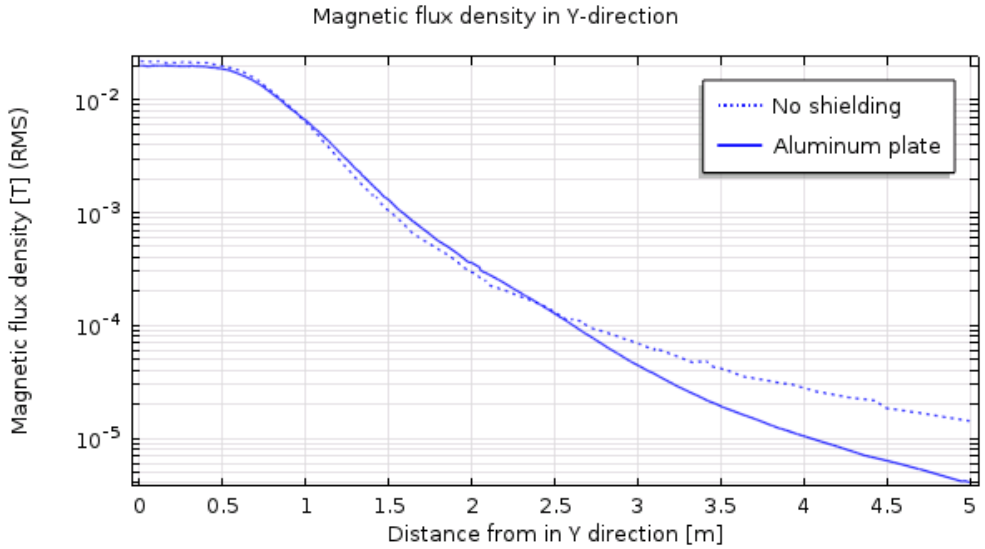

Figure 5.31 - Plot of magnetic flux density on Y-axis.

The numerical plot of the field in Y-direction indicates that the field is reduced from 2.5 meters off the center of the IPT and outwards. It also reduces the field between

sending and receiving end, which will to some extent reduce the efficiency of the power transfer.

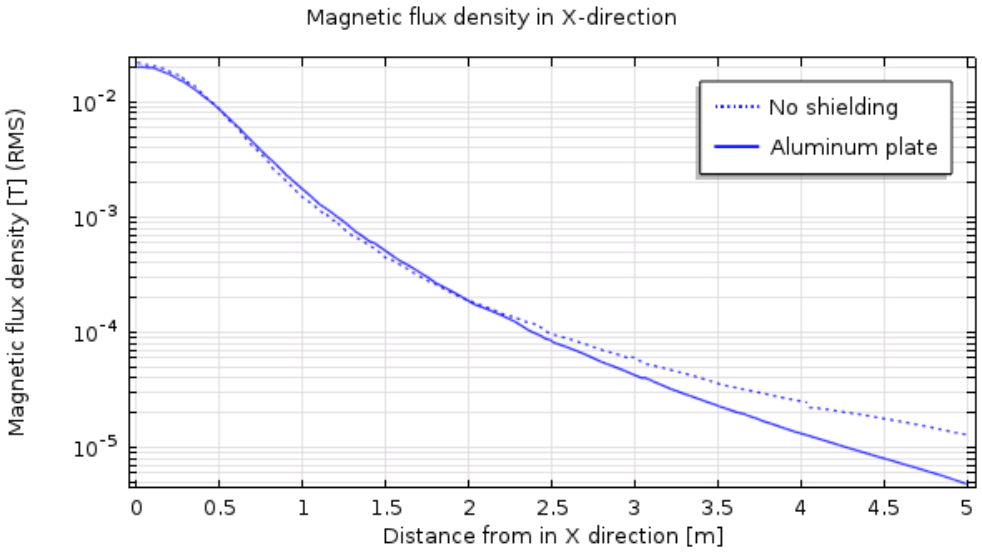

Figure 5.32 - Plot of magnetic flux density on X-axis.

Also in horizontal direction, X-axis the field is clearly reduced with the aluminum plate.

It seems clearly that the ship side, as long as the dimensions are large enough, is sufficient to keep the magnetic field from the IPT from penetrating in to the ship. The losses in the aluminum side of the ship are also very low, only 390 W compared to the power transfer, which is 1 MW.

5.5.3. Shielding added to sending end

A screen surrounding the sending end is added which should help reducing the magnetic field leaked to the surroundings, at least in the vertical and horizontal direction (Y and X axes).

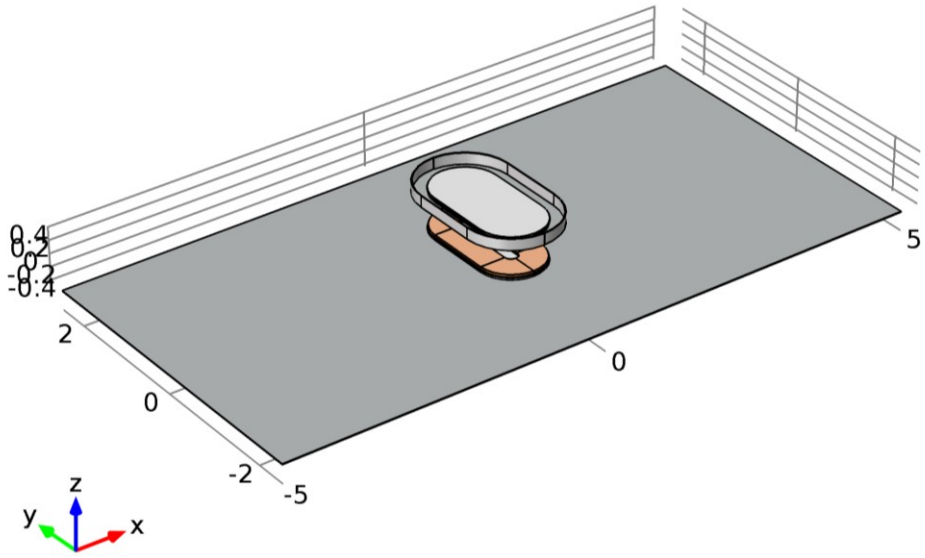

Figure 5.33 - Shielding added around sending end coil.

The magnetic flux density is plotted focusing in the range from 6 – 30 µT in Figure 5.34 for Z-Y axes and Figure 5.35 for Z-X axes. Comparing this configuration with only the aluminum plate (ship side) it shows that adding a shielding around the sending end reduces the field significantly. The losses, however increases because the EMF in the near field region is quite powerful and will induce strong currents in the shielding.

Losses
Plate: 841.03 W
Upper screen: 1971.30 W
Total: 2814.33 W

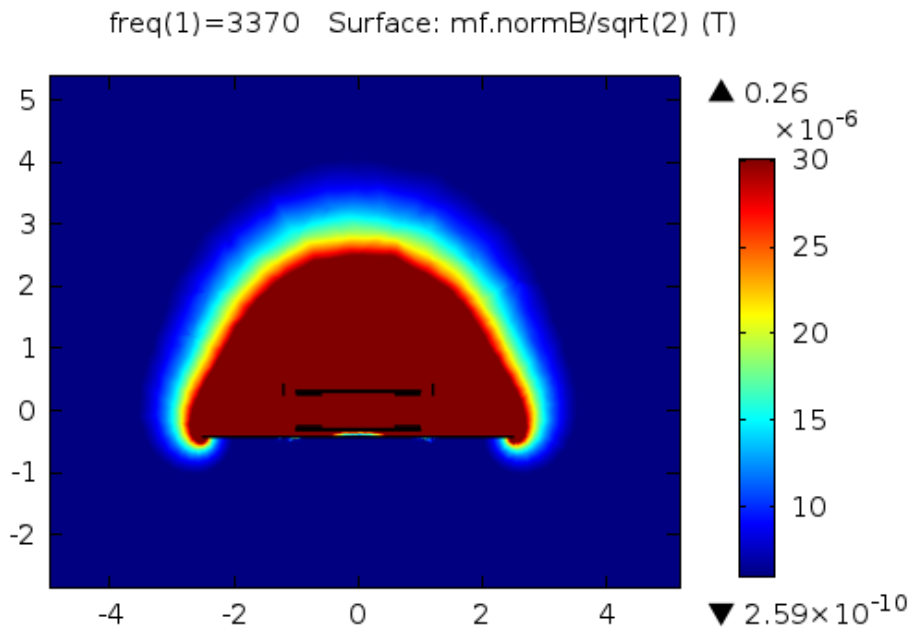

Figure 5.34 – Plot of magnetic flux density on Z-Y axes with aluminum screen added to sending end focusing in the range from 6 – 30 µT.

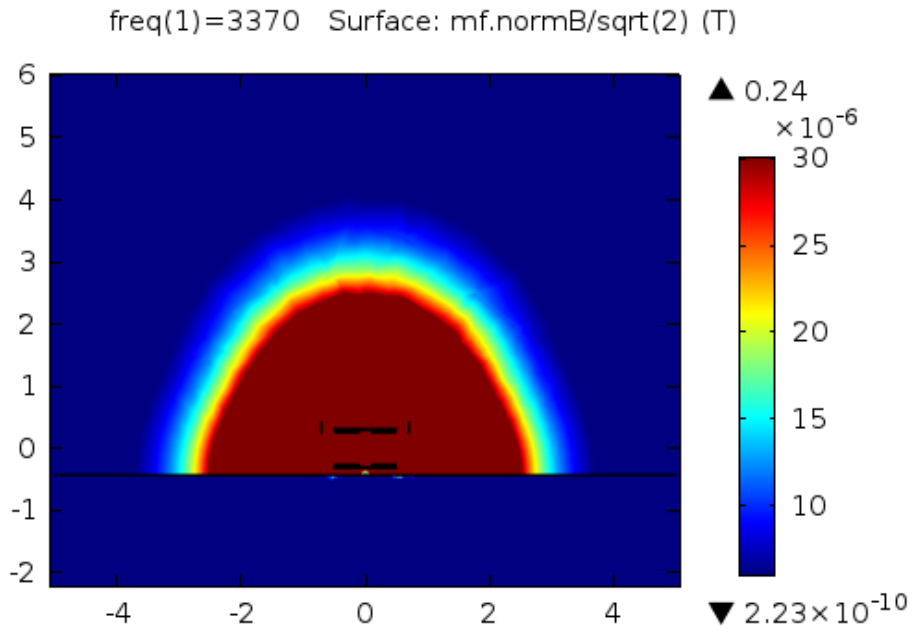

Figure 5.35 - Plot of magnetic flux density on Z-X axes with aluminum screen added to sending end focusing in the range from 6 – 30 µT.

5.5.4. Shielding added to sending and receiving end

A screen surrounding receiving end is also added as shown in Figure 5.36, but the effect of this, as shown in figures Figure 5.37 and Figure 5.38 is minimal. Only losses increase slightly.

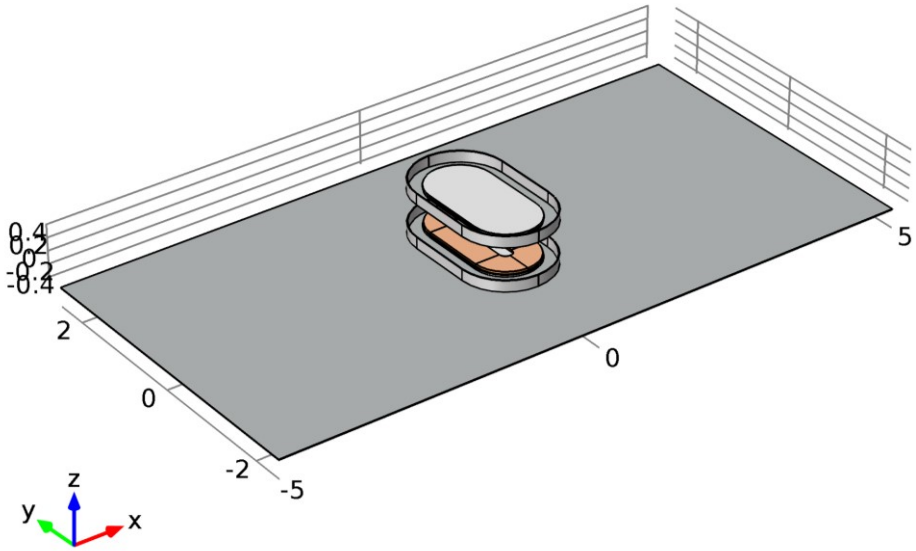

Figure 5.36 - Ship side with sending and receiving end shielding.

As shown in figures Figure 5.37 and Figure 5.38, simply adding a screen to sending end has little effect on the field, but this could also be expected seen out of the 2D simulation described in section 5.4.2. The losses however, increase significantly.

Losses
Plate: 392.8
Upper screen: 1749.35
Lower screen: 1200.27
Total: 3342.61

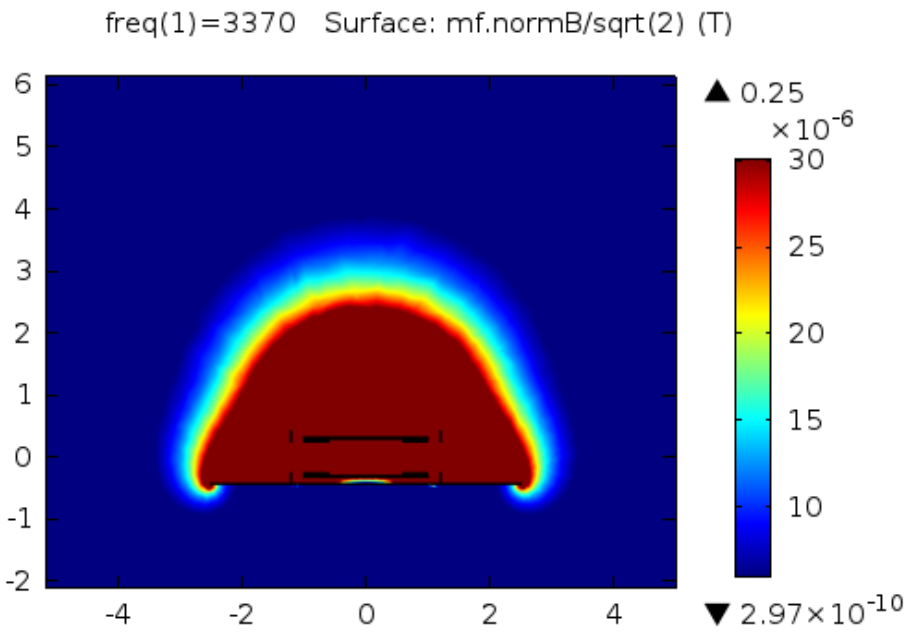

Figure 5.37 - Plot of magnetic flux density on Z-Y axes with aluminum screen added to sending and receiving end focusing in the range from 6 – 30 µT.

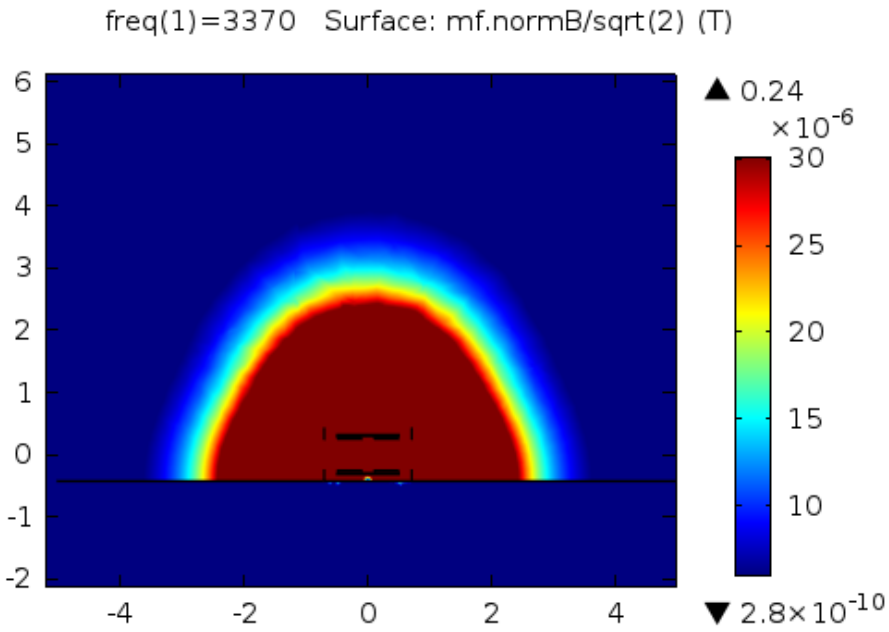

Figure 5.38 - Plot of magnetic flux density on Z-X axes with aluminum screen added to sending and receiving end focusing in the range from 6 – 30 µT.

5.5.5. Shielding applied to sending end and receiving end recessed in ship side

By sinking the receiving end coil down in the ship hull the shielding effect of the ship aluminum side should improve because it reduces the space where the field can be spread. Refer to Figure 5.39 for illustration.

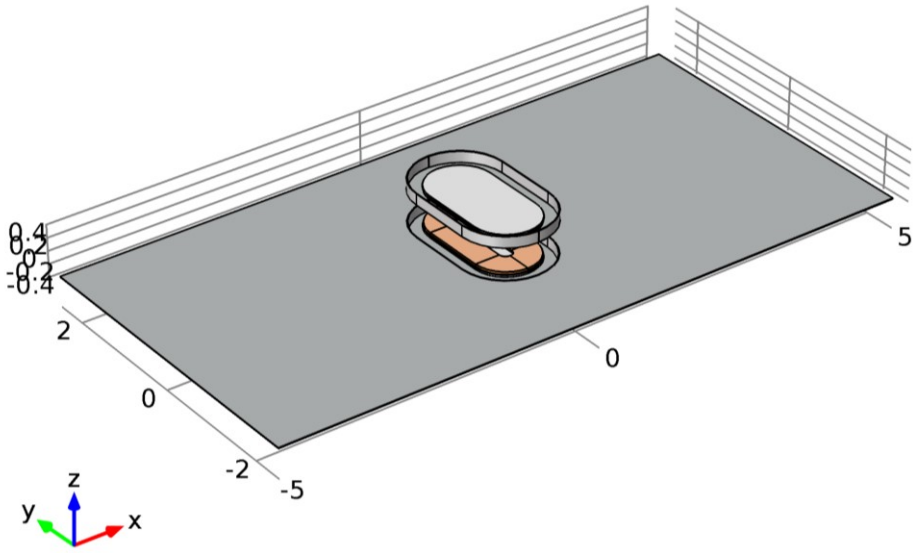

Figure 5.39 – Shielding around sending end and receiving end is recessed in to ship.

This configuration reduces the leakage field, but not by much as shown in figures Figure 5.40 and Figure 5.41. The losses are also slightly increased compared to the configuration where the IPT is not recessed and the shielding mounted on the aluminum.

Losses
Lower plate: 1706.87 W
Upper screen: 1704.24 W
Total: 3411.11 W

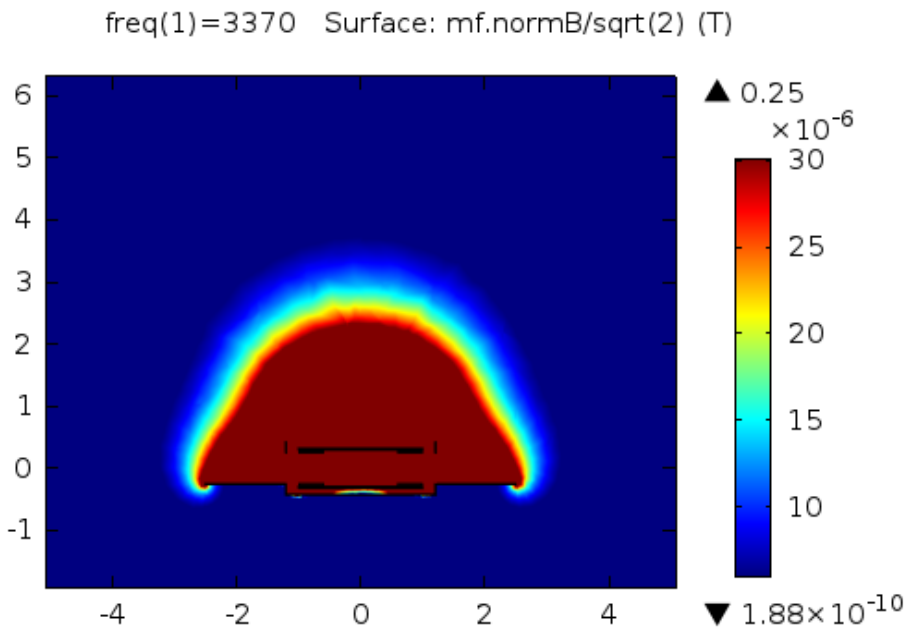

Figure 5.40 - Plot of magnetic flux density on Z-Y axes with shielding around sending end and receiving end recessed in to ship, focusing in the range from 6 – 30 µT.

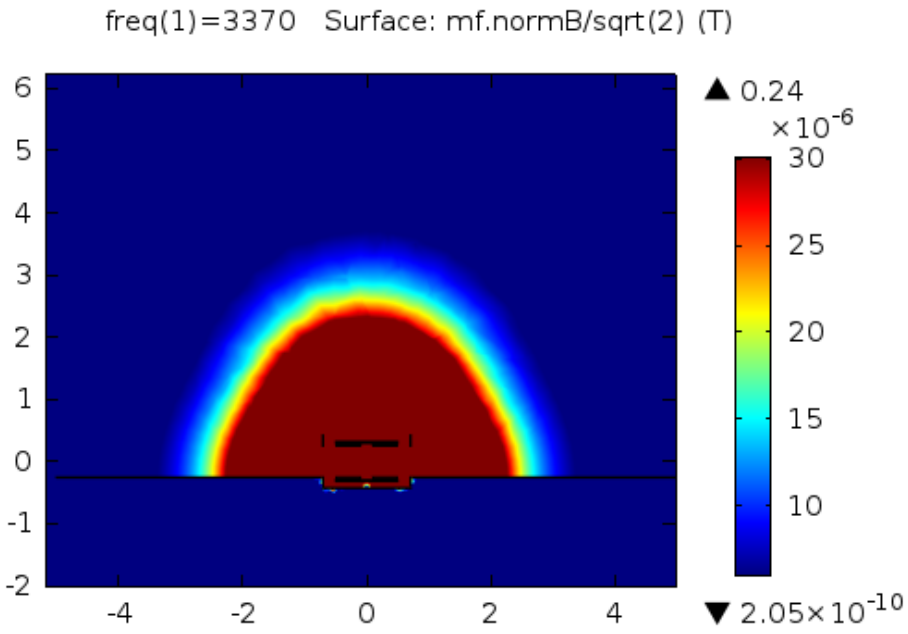

Figure 5.41 - Plot of magnetic flux density on Z-X axes with shielding around sending end and receiving end recessed in to ship, focusing in the range from 6 – 30 µT.

5.5.6. Enclosed shielding applied to sending end and receiving end recessed in ship side

By adding an upper screen to sending end as shown in Figure 5.42 the field should be more constrained in Z-direction as shown in the 2D simulations from section 5.4.7.

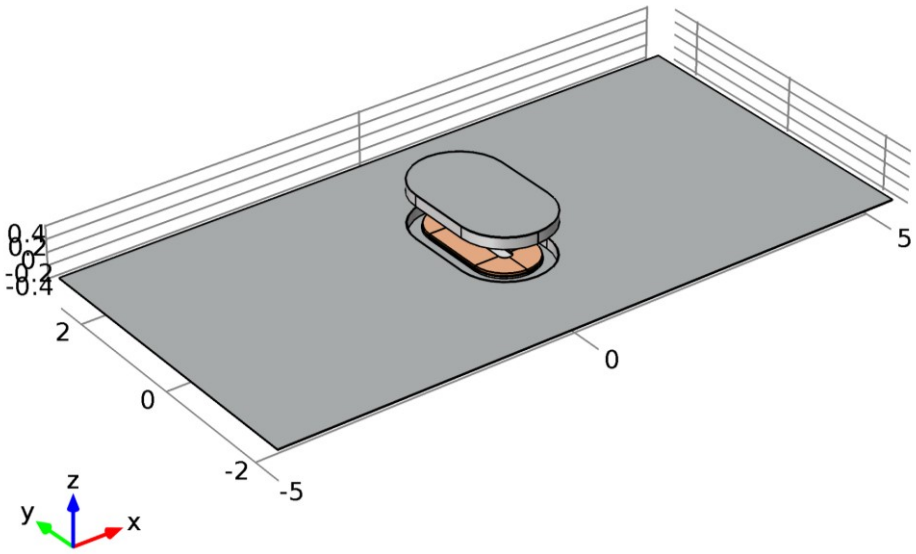

Figure 5.42 – Enclosed shielding around sending end and receiving end is recessed in to ship.

The 2D plots from the 3D simulation in figures Figure 5.43 and Figure 5.44 are easily recognizable with the plot shown in Figure 5.20. The leakage field is reduced significantly and the losses are also decreased.

Losses
Lower plate: 1687.11
Upper screen: 1640.60
Total: 3327.70

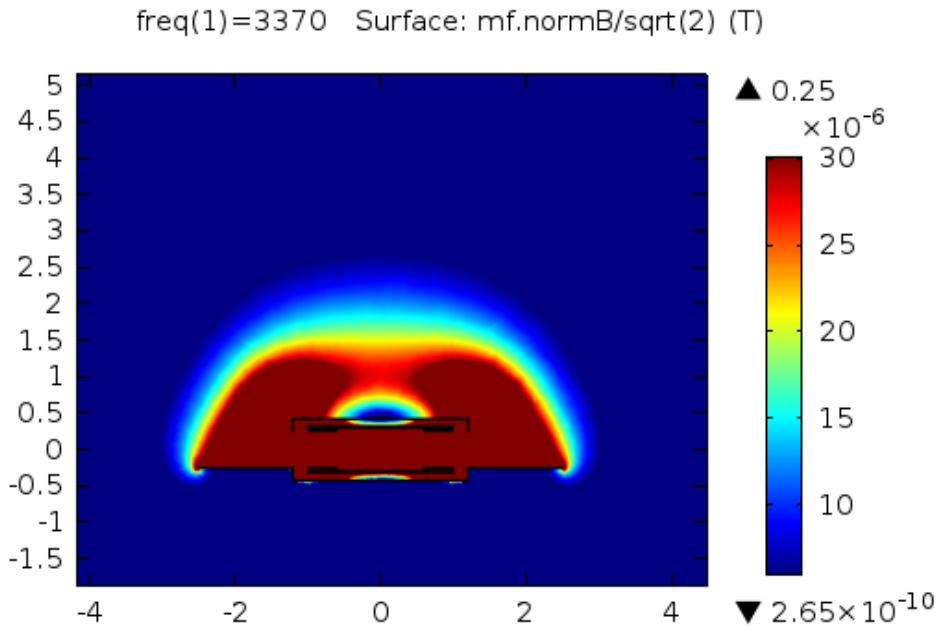

Figure 5.43 - Plot of magnetic flux density on Z-Y axes with enclosed shielding around sending end and receiving end recessed in to ship, focusing in the range from 6 – 30 µT.

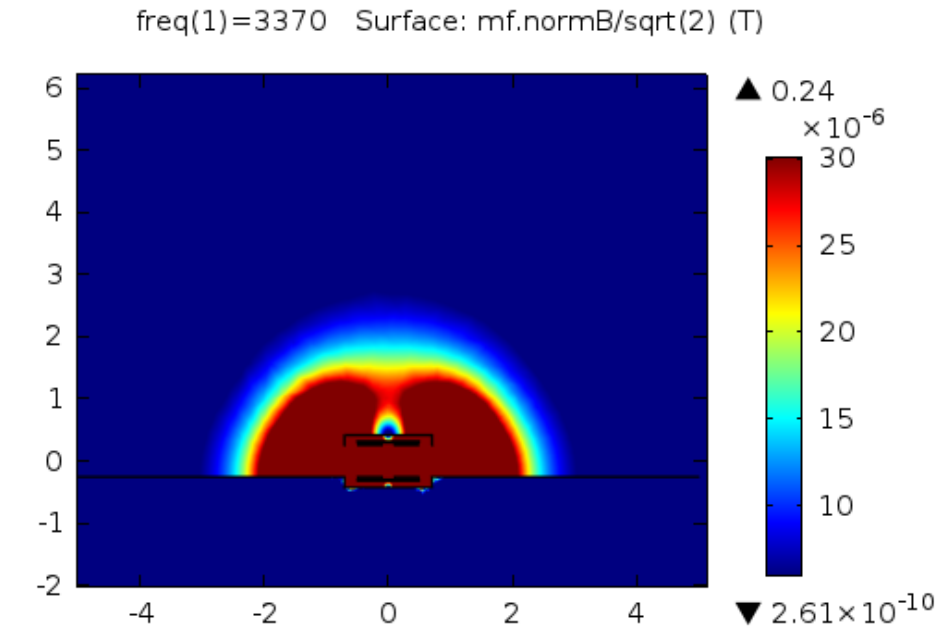

Figure 5.44 - Plot of magnetic flux density on Z-X axes with enclosed shielding around sending end and receiving end recessed in to ship, focusing in the range from 6 – 30 µT.

5.5.7. Enclosed and extended screen applied to sending end and receiving end recessed in ship side

An extending plate like the one on ship side is added to sending end. This is probably the best shielding option possible, and further from this configuration only the dimensions of the aluminum plates can be increased. As mentioned above this is probably a very conservative estimate of the size of the ship side, and for the final construction it will most likely be larger.

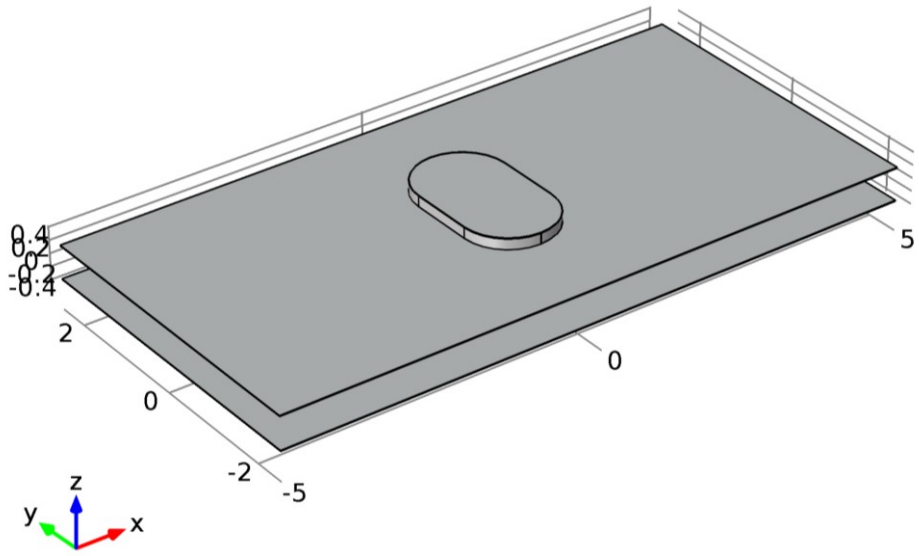

Figure 5.45 - Sending end is applied with the same shielding as receiving end.

The simulation results showing the flux density plotted in figures Figure 5.46 and Figure 5.47 shows that the leakage field now is very constrained. The losses are also reduced compared to the previous simulation.

Losses
Lower plate: 1628.20
Upper plate: 1628.20
Total: 3250.40

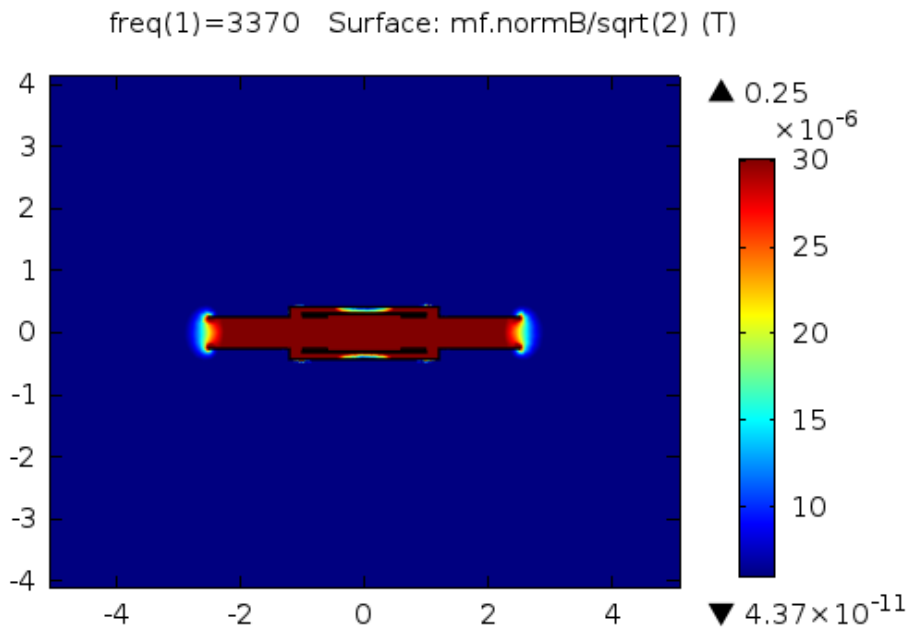

Figure 5.46 - Plot of magnetic flux density on Z-Y axes with enclosed and extended shielding around sending end and receiving end recessed in to ship, focusing in the range from 6 – 30 µT.

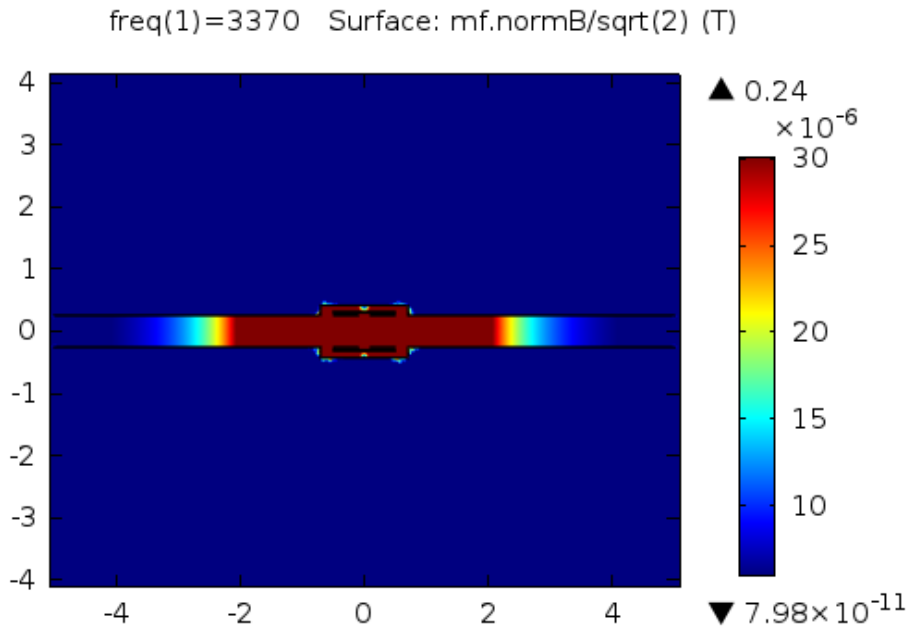

Figure 5.47 - Plot of magnetic flux density on Z-X axes with enclosed and extended shielding around sending end and receiving end recessed in to ship, focusing in the range from 6 – 30 µT.

5.5.8. Numeric plots of shielding configurations

The simulation results from all 3D tests are plotted numerically on axes with origin at the center of the model shown in figures Figure 5.28 and Figure 5.29. These plots for Y, X and Z –axes can be seen respectively in figures Figure 5.48, Figure 5.49 and Figure 5.50. From the plots it seems that the most effective shielding is the ship side itself in addition to some shielding around the sending end. Other measures beyond this have lower effect individually, but all combined seems to be more significant.

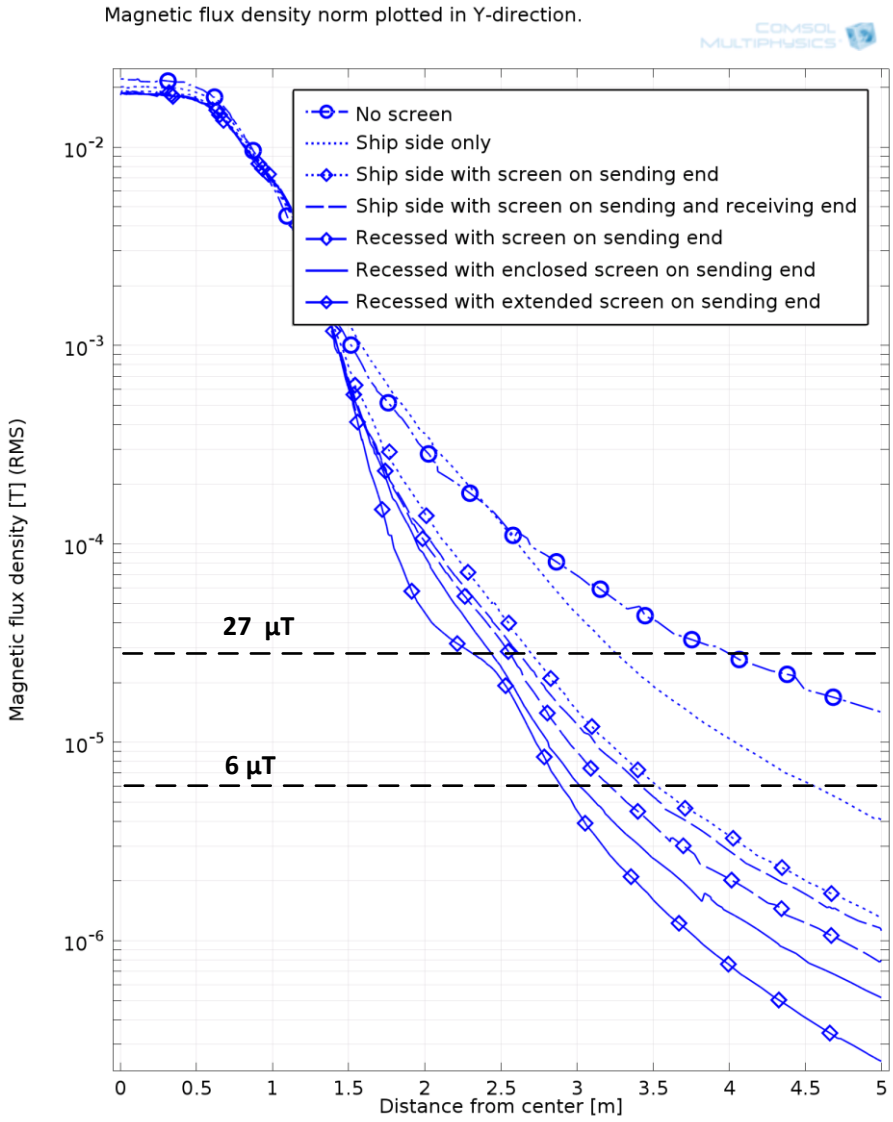

Figure 5.48 - Numerical plot of magnetic flux density along Y-axis for various shield configurations.

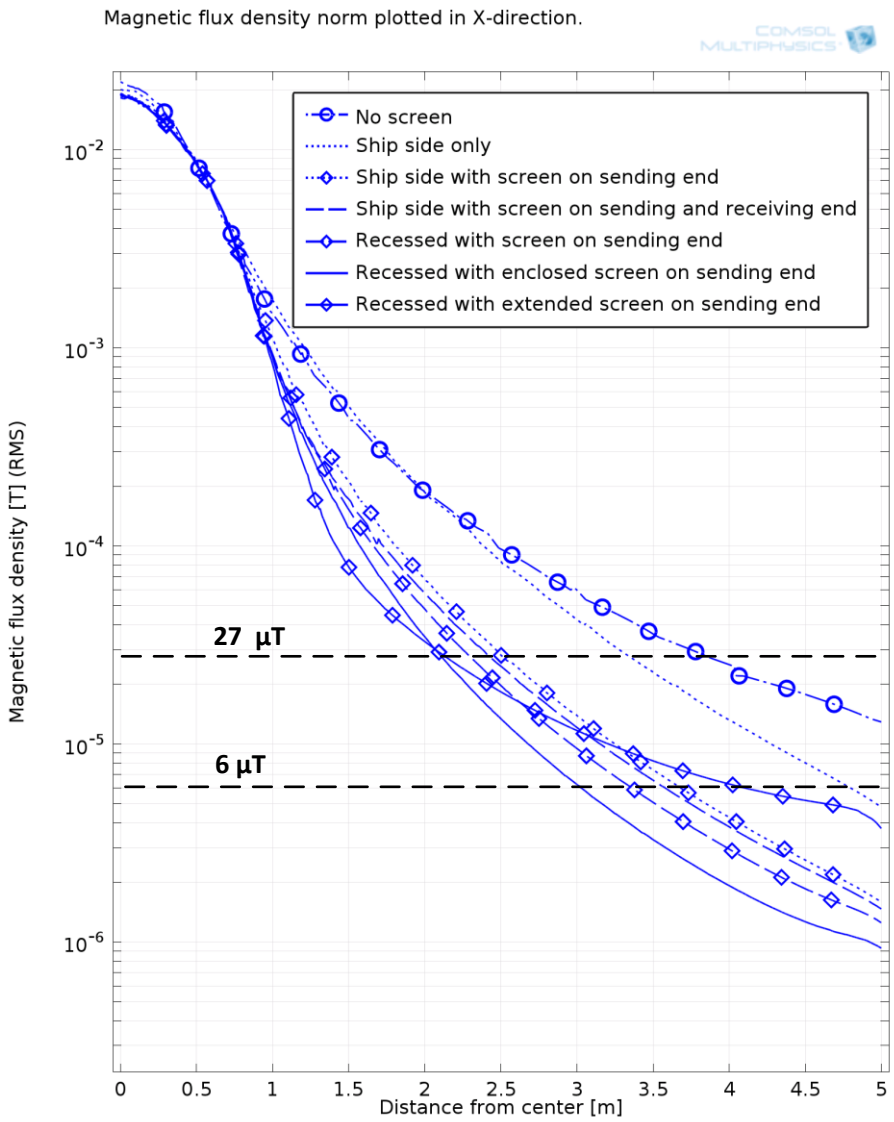

Figure 5.49 - Numerical plot of magnetic flux density along X-axis for various shield configurations.

The leakage flux along X-axis seems to be a little higher than for Y-axis.

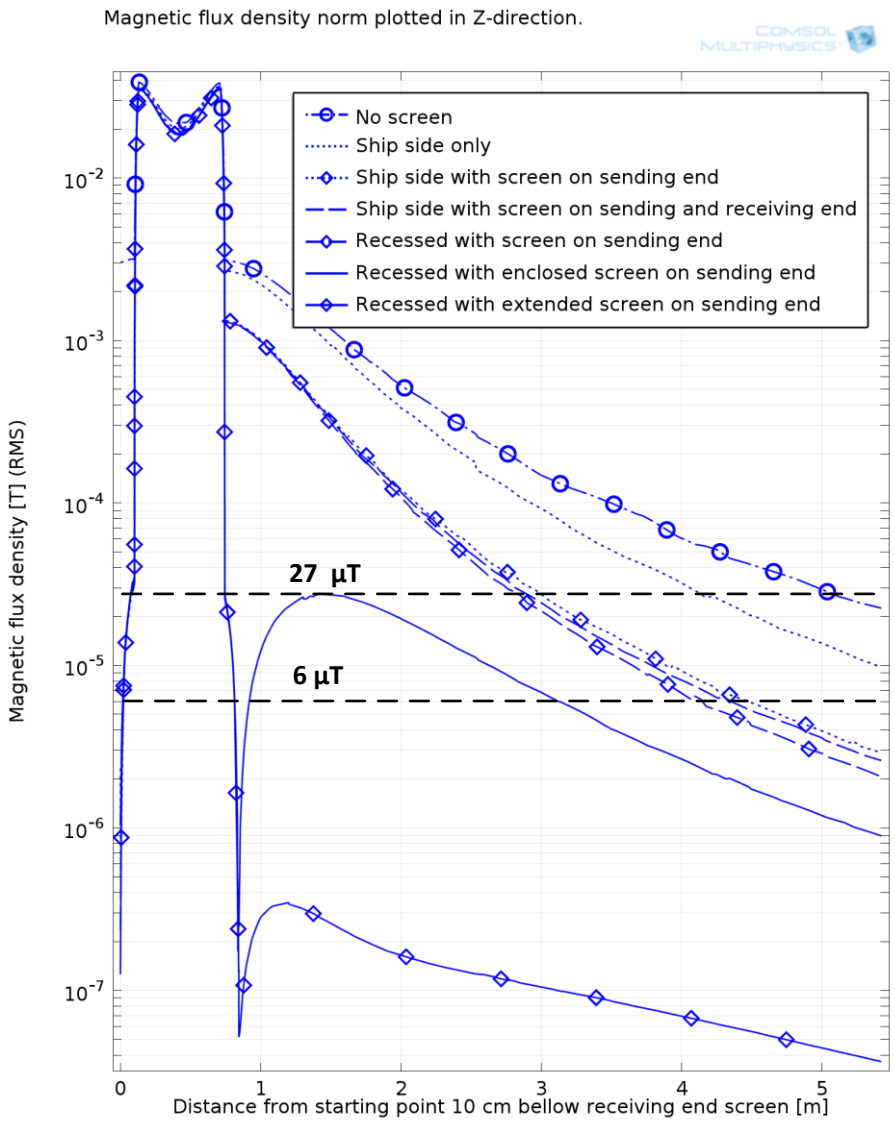

Figure 5.50 - Numerical plot of magnetic flux density along Z-axis for various shield configurations.

Along the Z-axis the most effective shielding appears to be the configurations where the sending end is enclosed.

5.6. 3D models with misalignment

Since the IPT system is supposed to be fitted on ferries a certain degree of misalignment can be expected because of the ships movement in the sea. Some of the 3D simulations shown in section 5.5 are now tested with misalignment between sending and receiving end. Specifically the misalignment in per unit for this case is given in [1] as:

$$dy_{pu} = \frac{dy}{Lenght/2} \tag{5.1}$$

where dy is the actual misalignment which is 0.707 p.u. and the gap length is reduced to 0.3 so that the same coupling coefficient (rate of power transfer) described in [1] remains almost the same.

5.6.1. No shielding

Misalignment is simulated with no shielding applied to compare the flux density with the coils aligned, and the flux density is plotted in Figure 5.51 which can be compared with Figure 5.26 (a).

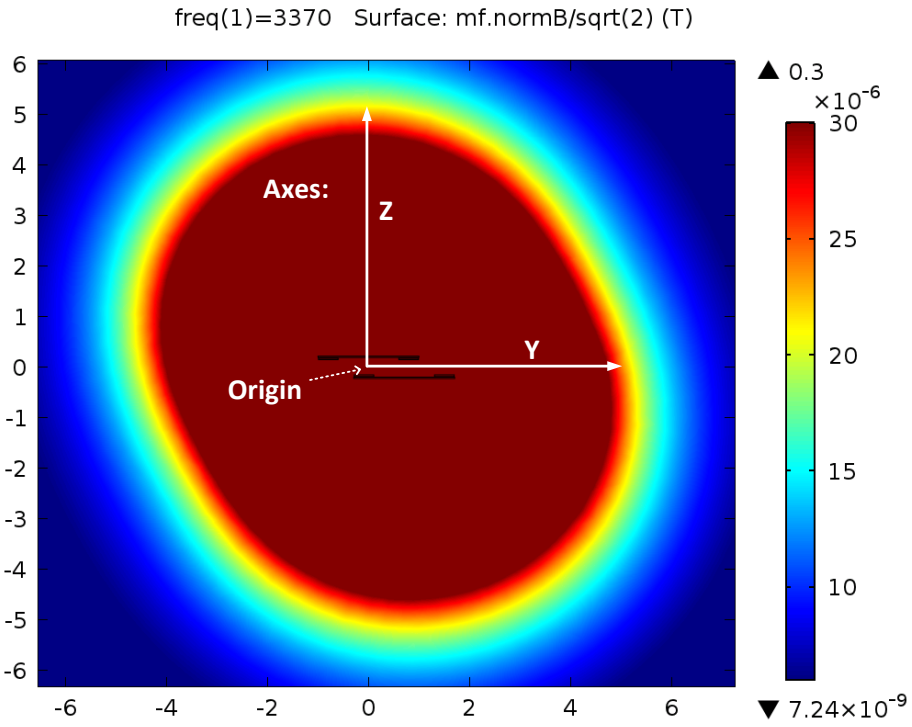

Figure 5.51 - Plot of magnetic flux density on Z-Y axes with coils misaligned and no shielding, focusing in the range from 6 – 30 µT.

The difference in magnetic flux density between aligned coils and misaligned coils can be seen out of the plot shown in Figure 5.52 where the flux density as function of distance from a specified origin as drawn in Figure 5.51 is plotted numerically.

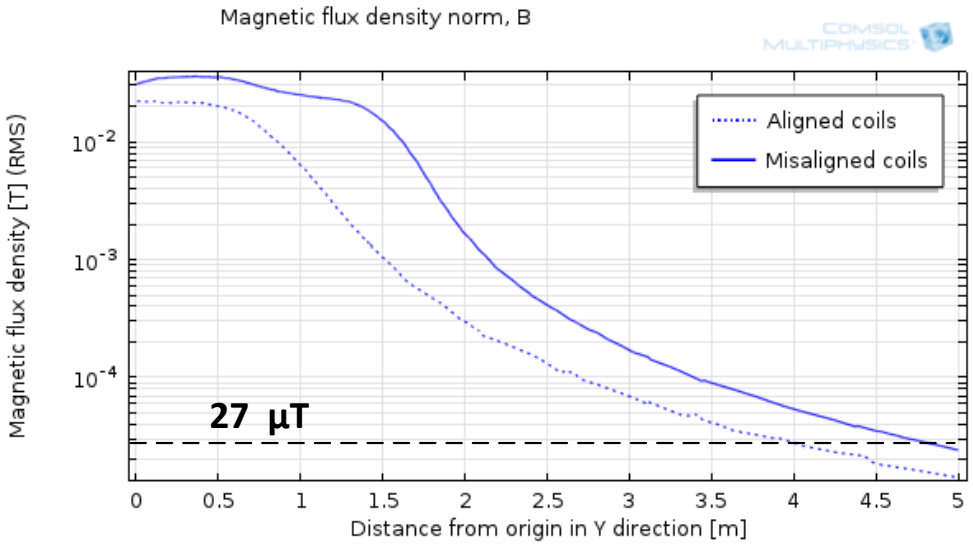

Figure 5.52 – Numerical plot of magnetic flux density in specified Y-direction with no shielding applied, comparing aligned coils against misalignment.

As could be expected, the difference is at the largest at 1.5 meters from the origin because the receiving end would be right at this point.

5.6.2. Aluminum ship side

The ships aluminum side is applied behind the receiving end to study misalignment where magnetic flux density is plotted in Figure 5.53.

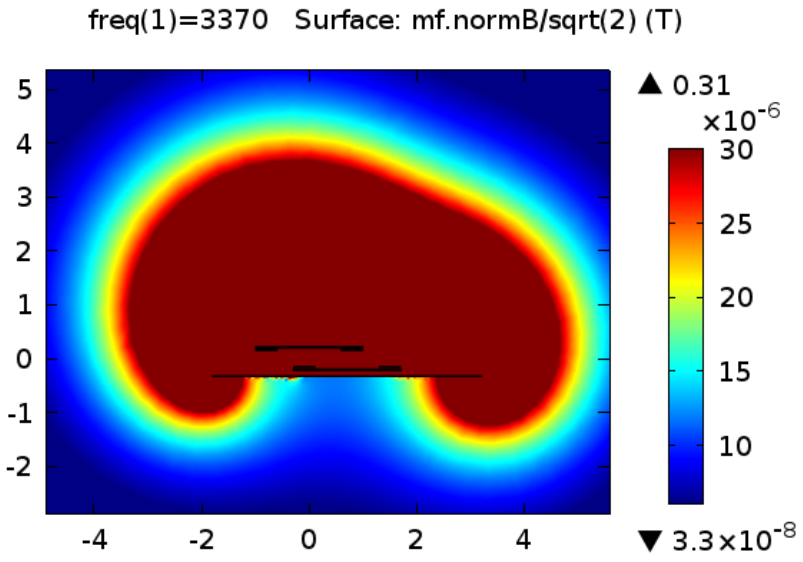

Figure 5.53 - Plot of magnetic flux density on Z-Y axes with coils misaligned and ship aluminum side, focusing in the range from 6 – 30 µT.

By comparing coils misalignment with aligned coils as shown in Figure 5.28 it seems clear that the misalignment between sending and receiving end increases the field leakage quite significantly, despite the shielding from the ship. This also clearly shows in the numerical plot of magnetic flux density as function of distance from the origin specified in Figure 5.54. Losses are increased by approximately 1 kW.

Plate losses: 1295.54 W

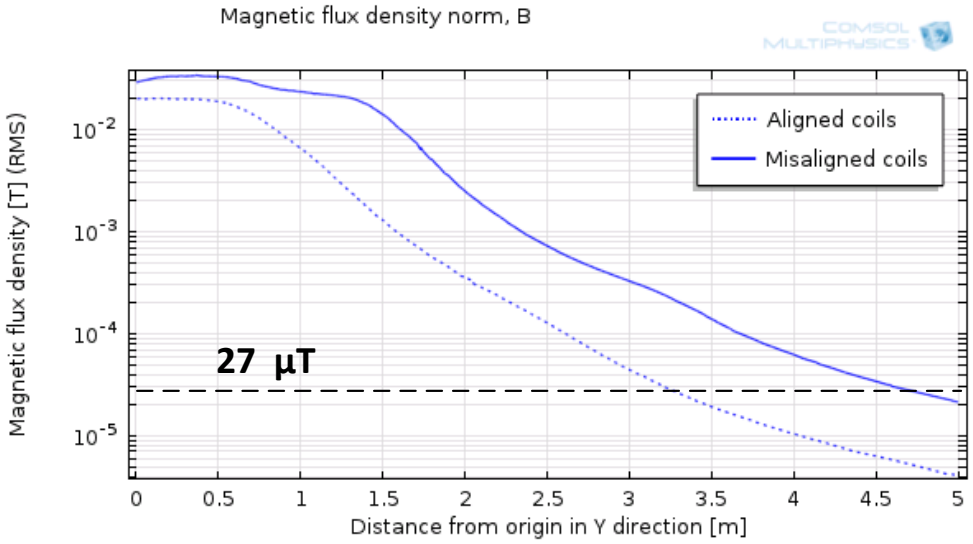

Figure 5.54 - Numerical plot of magnetic flux density in specified Y-direction with aluminum ship side, comparing aligned coils against misalignment.

5.6.3. Shielding applied to sending end

By adding shielding to sending end the field emitted from the IPT would be expected to decrease as it does when the coils are aligned, but by comparing the plot in Figure 5.55 with Figure 5.53 it seems that the total field strength in Y-direction remains more or less the same. The field in Z-direction is slightly reduced.

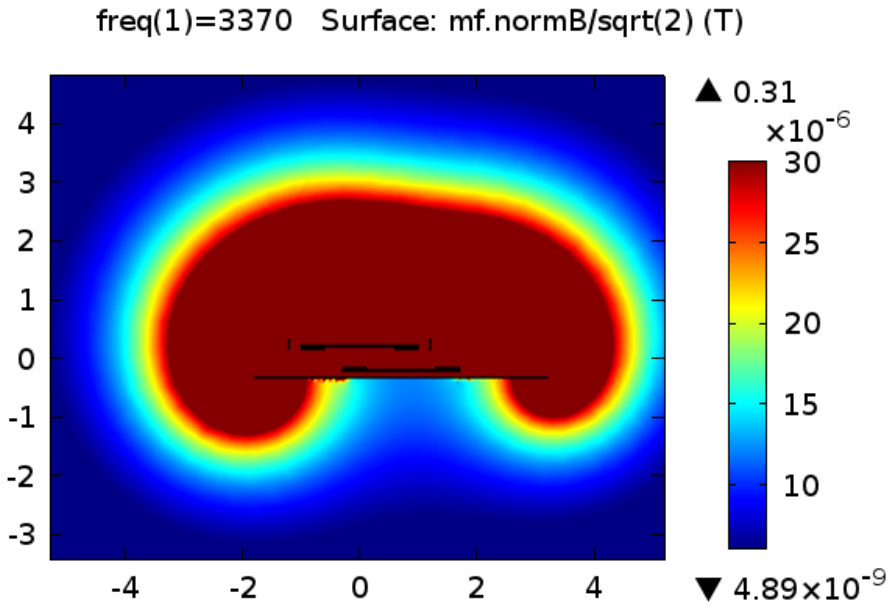

Figure 5.55 - Plot of magnetic flux density on Z-Y axes with coils misaligned and ship side with shielding applied to sending end, focusing in the range from 6 – 30 µT.

The field strength in Y-direction is plotted numerically in Figure 5.56, and by comparing this to the plot in Figure 5.34, it confirms that the flux density does not change by any significance. In other words, this shielding configuration is not doing much to reduce the field with this misalignment.

Losses
Upper screen: 2420.18 W
Plate: 1058.12 W
Total: 3478.31 W

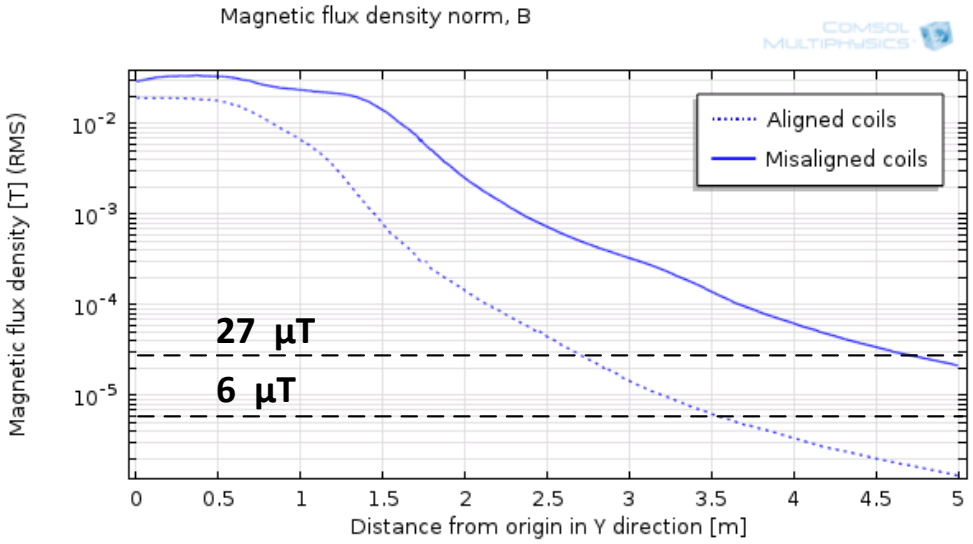

Figure 5.56 - Numerical plot of magnetic flux density in specified Y-direction with shielding applied to sending end, comparing aligned coils against misalignment.

5.6.4. Shielding applied to sending end and receiving end recessed in ship side

Simulation with the receiving end recessed in to the ship and with sending end shielding added are performed, and result is plotted in Figure 5.57. As can be seen from the plot, this makes some reduction to the field strength.

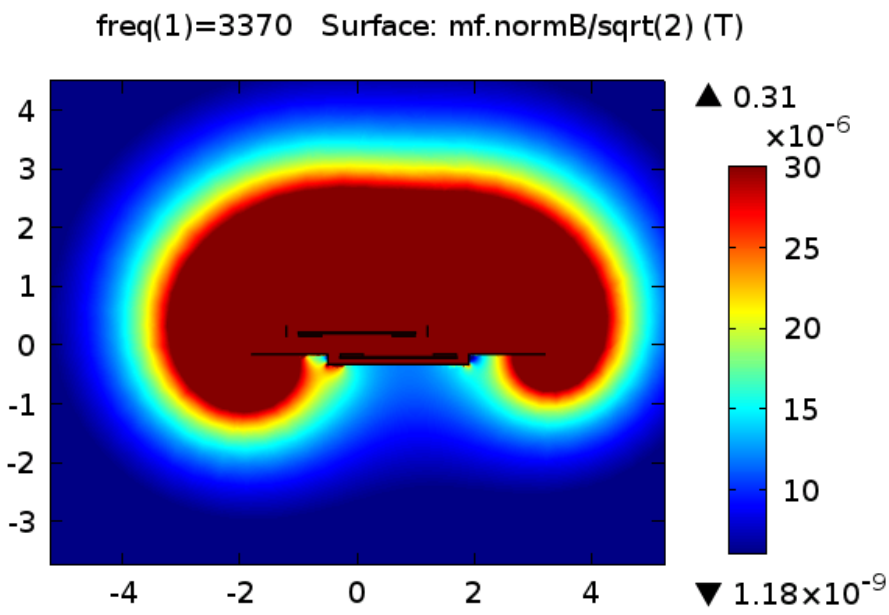

Figure 5.57 - Plot of magnetic flux density on Z-Y axes with coils misaligned, receiving end recessed in ship side and shielding applied to sending end, focusing in the range from 6 – 30 µT.

A numerical plot of the magnetic flux density, which is plotted in Figure 5.58 shows that it is now almost down to 10 µT at five meters away from the center of the IPT.

Losses
Upper screen: 2095.46
Plate: 2367.88
Total: 4463.34

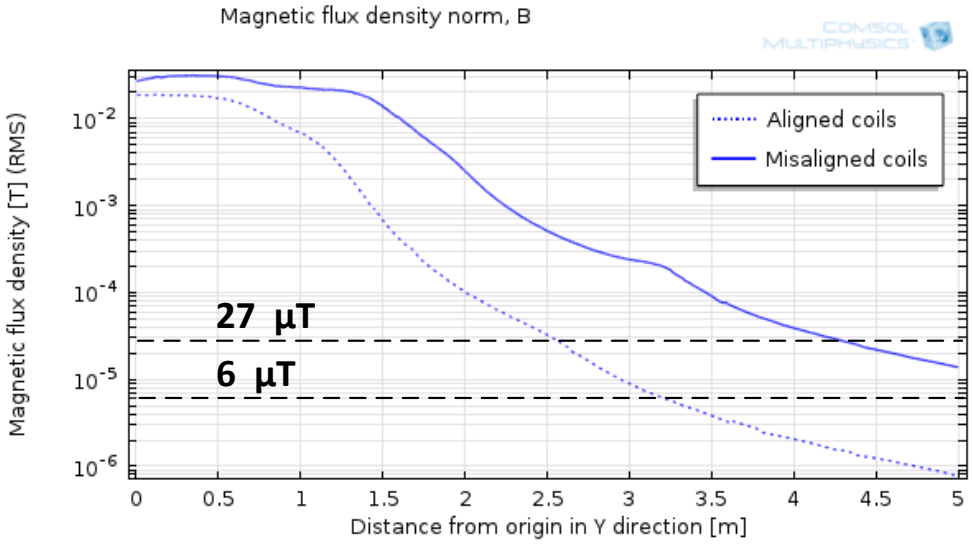

Figure 5.58 - Numerical plot of magnetic flux density in specified Y-direction with shielding applied to sending end and receiving end recessed in ship side, comparing aligned coils with misalignment.

5.6.5. Enclosed shielding applied to sending end and receiving end recessed in ship side

Adding a rear shielding to sending end should, just like the model discussed in section 5.5.6 reduce the leakage field in Z-direction. The simulation result is shown in Figure 5.59.

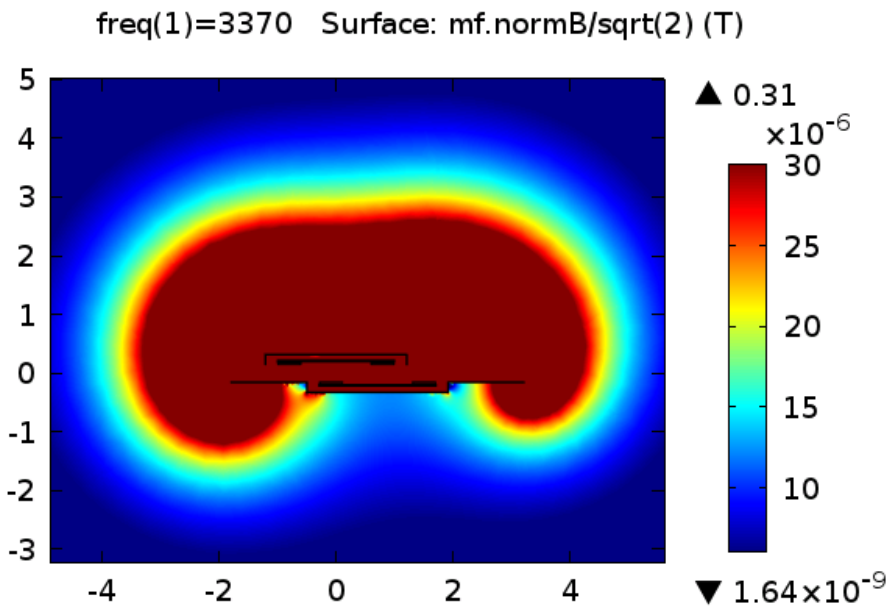

Figure 5.59 - Plot of magnetic flux density on Z-Y axes with coils misaligned, receiving end recessed in ship side and enclosed shielding applied to sending end, focusing in the range from 6 – 30 µT.

The result shows that with misalignment, a shielding plate at the rear of the sending end has little effect. Only the flux density in region around 4 meters in z-direction is slightly reduced, but in the numerical plot in Figure 5.60 shows that it has almost no effect in Y-direction. Losses are a little reduced.

Losses
Upper screen: 2056.25
Plate: 2314.22
Total: 4370.46

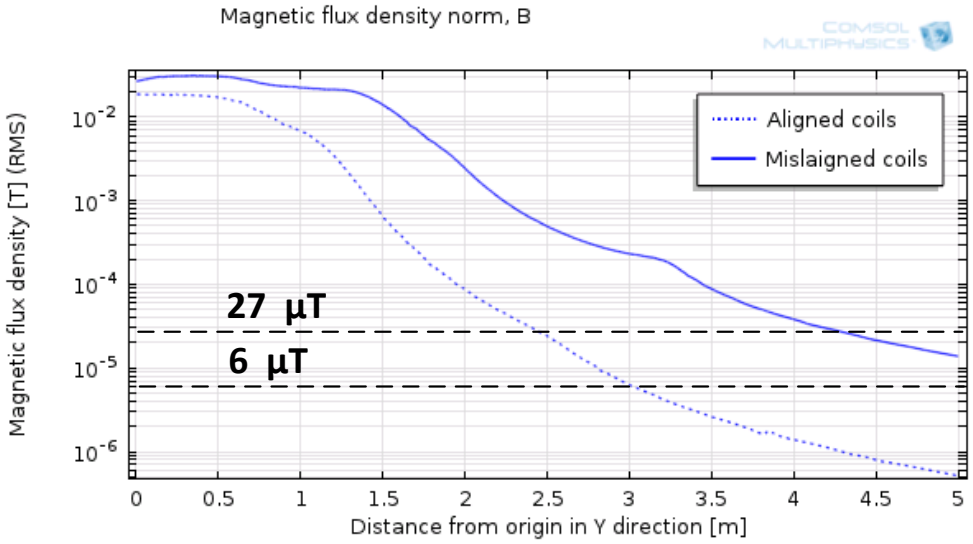

Figure 5.60 - Numerical plot of magnetic flux density in specified Y-direction with receiving end recessed in ship side and enclosed shielding applied to sending end, comparing aligned coils against misalignment.

5.6.6. Enclosed and extended screen applied to sending end and receiving end recessed in ship side

Enclosed and extended shielding is tested with misalignment, and plot is shown in Figure 5.61.

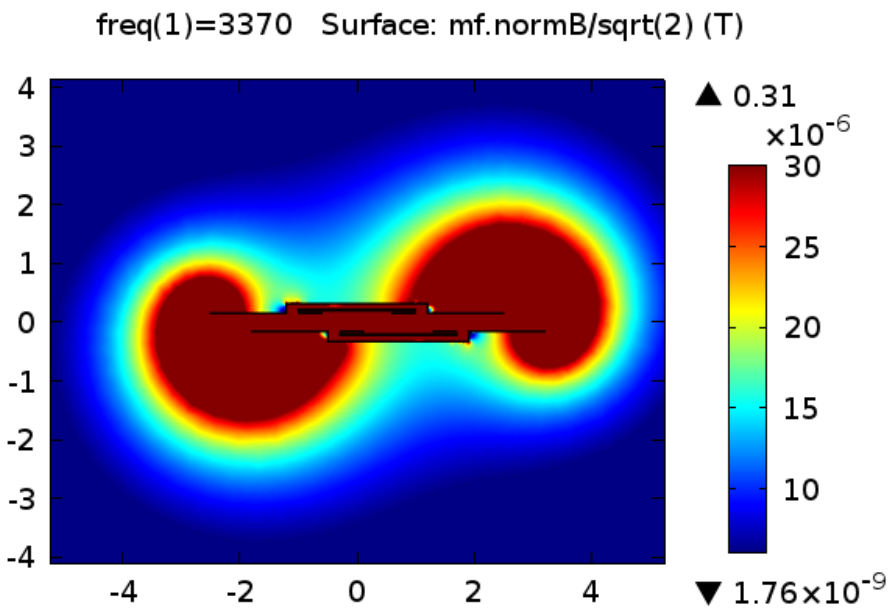

Figure 5.61 - Plot of magnetic flux density on Z-Y axes with coils misaligned, receiving end recessed in ship side and enclosed extended shielding applied to sending end, focusing in the range from 6 – 30 µT.

Simulation shows that the leakage field reaches out about 4 meters in Y-direction, even with both sending and receiving end as much enclosed as possible.

Losses
Upper screen: 2241.80
Plate: 2234.30
Total: 4476.11

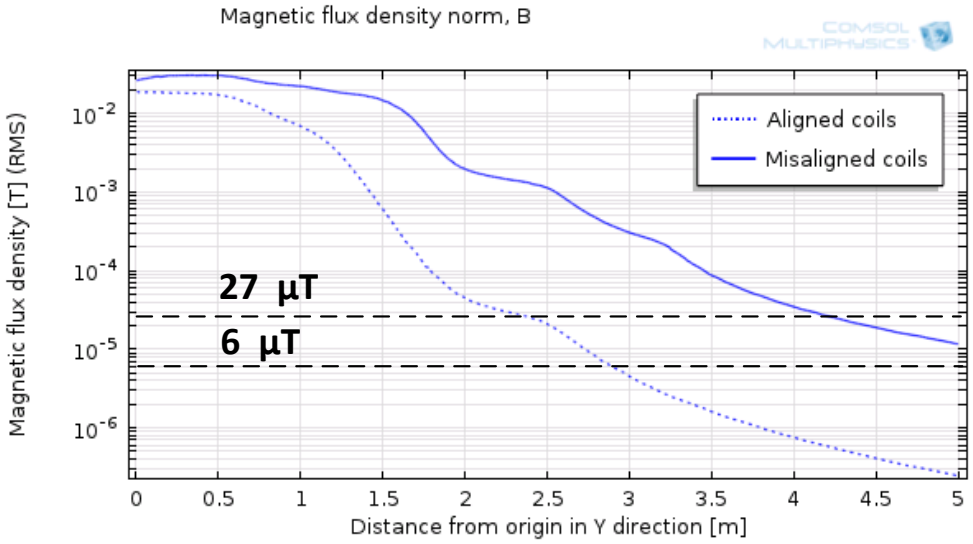

Figure 5.62 - Numerical plot of magnetic flux density in specified Y-direction with receiving end recessed in ship side and enclosed extended shielding applied to sending end, comparing aligned coils against misalignment.

5.6.7. Numeric plots of shielding configurations with misalignment

The shielding configurations from all simulations with misalignment are plotted numerically the same way as described in section 5.5.8.

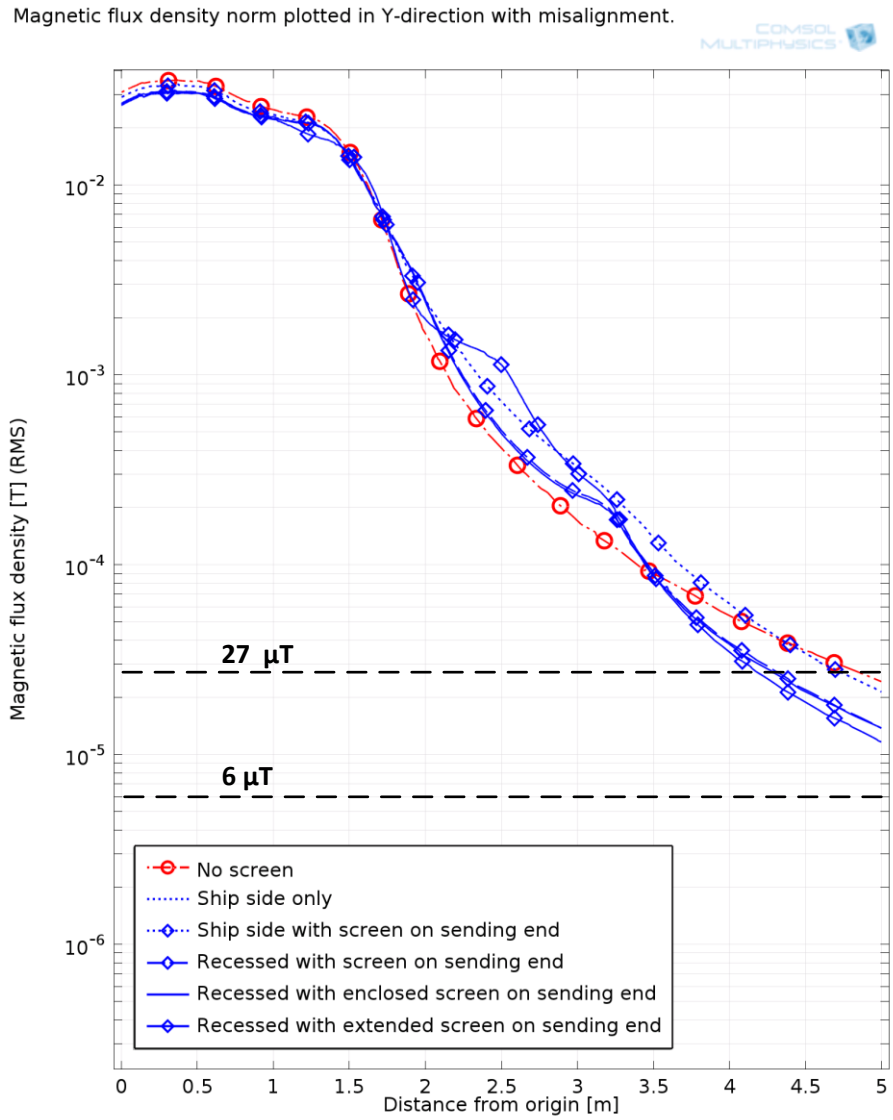

Figure 5.63 - Numerical plot of magnetic flux density along Y-axis for various shield configurations with misalignment.

By studying the numerical plot in Y-direction of magnetic flux density with misalignment it seems that having the receiving end recessed into the ship side is the best action for containing the leakage field.

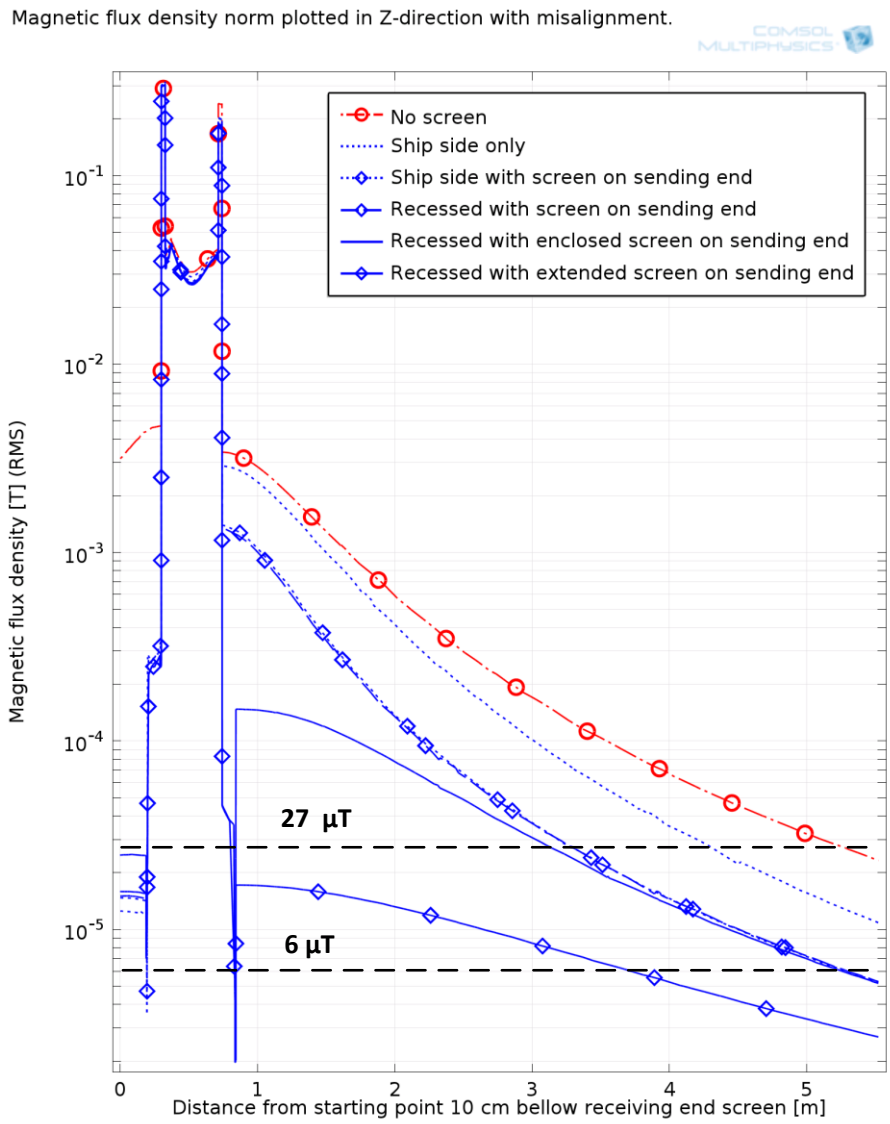

Figure 5.64 - Numerical plot of magnetic flux density along Z-axis for various shield configurations with misalignment.

By studying the numerical plot in Z-direction of magnetic flux density with misalignment it seems that shielding around the receiving end and especially enclosed shielding is the most effective action for containing the leakage field.

6. Discussion

COMSOL simulations compared to actual coil measurements

COMSOL Multiphysics is well-tested simulation software, but because of its complexity less experienced users should somehow try to have models and methods verified. There are especially some precautions that must always be taken when using COMSOL;

Before the field is evaluated, it should be verified that the coil has the correct current and current distribution which can be checked by doing analyses on current density. A multi turn coil domain can be modelled in four different ways. One must also consider that COMSOL always operate with amplitude values, and must correct for this before evaluating the field strength.

When doing physical measurements with an EMC field analyzer on electromagnetic fields there may be inaccuracy in the instrument, thus calibration reports should always be checked. Another source of error is if the instrument is not held in a correct position, even a few millimeters can affect the result severely.

Still, these examinations indicate that the method applied in COMSOL Multiphysics works fine for computing magnetic field distribution, also when there is shielding present.

COMSOL modelling of IPT

Simulations done in COMSOL Multiphysics have shown that 2D simulations can give a detailed picture on how magnetic field propagates from a coil. If the coil is not perfectly circular, the result from 2D axisymmetric will deviate from the actual coil depending on the size.

The results from 3D modelling show that it is possible to limit the magnetic leakage field by using various configurations of aluminum shielding around sending and receiving end coils. When misalignment occurs, the effect of the shielding is significantly reduced, but still it is possible to limit the field. The configuration of the shielding will depend on how much limitation of the EMF that is desirable and in turn, weighted against the amount of loss that can be tolerated. Generally, this report has only considered a few options based on the information that exists

about IPT at the moment, but more accurate tests should be performed as more exact data is available.

Other considerations when using FEM software

There are also some other considerations to be aware about when using FEM software. The meshing and the mesh size may have significant impact on the results. E.g. in some of the numerical plots in section 5.5.8 it is possible to see some irregularities in the graphs which can be explained by rough meshing in this area.

Another consideration is the size of the domain created for the simulation. If the domain is too small, the results will be inaccurate because of the boundary conditions. Domain for these simulations was a sphere with radius about 10 times larger than the IPT geometry. However, a large geometry is heavier to compute and will add time to complete a simulation.

Concerning materials, the permeability of ferrite is not constant. This however, should not have any effect when doing studies on the leakage field.

Personal skill and experience with COMSOL is also a factor. There are perhaps better ways of doing modelling than what has been done for this project.

Conclusion

This report has considered various types of shielding for the IPT system to create an overview of different options and the effect of these.

It has been referred to guidelines published by ICNIRP containing reference levels for the highest exposure levels of electromagnetic field strength for general public and occupational personnel. In addition it has been verified that the NRPA puts these guidelines as a basis for the levels of electromagnetic radiation that can be allowed for use in public areas, although individual assessments must be carried out for each facility.

Experiments on a coil and COMSOL modelling of this coil with and without shielding has indicated that the method applied in this project for modelling the IPT system will give results very close to the actual values. The COMSOL modelling of the IPT system has given a good approximation on what to be expected regarding how the EMF spreads out to the area around the system depending on alignment and shielding.

The IPT system with the configurations considered in this case will, out to a distance of 5-6 meters proses magnetic field strength above the reference levels given in the ICNIRP guidelines, but it can be significantly reduced by use of shielding. Conclusively, the leakage field produced by the IPT is manageable and should not be of any problem with respect to the implementation of this system. Regarding misalignment there are some challenges, but a recessed receiving end, as well as shielding around sending end will help contain the leakage field.

Further work

The models of the IPT system considered in this report are only a small selection of all possible opportunities, both regarding the configurations of the IPT itself and the shielding configurations. Also, the models are very basic with focus on the magnetic field and flux density only. For further work, these models could be extended to include physics on heat transfer and electrostatics in addition to magnetic fields. Different materials could be considered as well. When a full scale prototype of the IPT is built, the simulations made in this report should also be verified by field measurements.

This study has only included a small part of the total IPT system. There are also other studies that could be done, like how a sudden power transfer of 1 MW would impact on the local grid and the power stability, or how the batteries on a ferry would cope with such fast charging.

Bibliography

[1] G. Guidi, "Induction Power Transfer, Project number: 502000114," SINTEF, Trondheim, 2013.

[2] Y. Shangzun, "Study on Electromagnetic Radiation of Ultra-High Voltage Power Transmission Line," IEEE, Singapore, 2008.

[3] A. Anany, "Radiation exposure from electric power lines and methods for reducing the magnetic field generated by distribution network," IET, Stockholm, 2013.

[4] United States environmental protection agency, "EPA," United States environmental protection agency, 17 05 2013. [Online]. Available: http://www.epa.gov/radiation/understand/ionize_nonionize.html#nonionizing. [Accessed 26 05 2014].

[5] Norwegian ministery of health and care services., "Lovdata," 2010. [Online]. Available: http://lovdata.no/dokument/SF/forskrift/2010-10-29-1380#KAPITTEL_5. [Accessed 7 Mars 2014].

[6] ICNIRP, "Gidelines for limiting exposure to time-varying electric, magnetic, and electromagnetic fields (Up to 300 GHz)," Health Physics Society, 1997.

[7] SuperManu, "Wikipedia," Wikimedia Commons, 03 06 2014. [Online]. Available: http://en.wikipedia.org/wiki/Electromagnetic_radiation. [Accessed 03 06 2014].

[8] R. D. Saunders, Biological effects of exposure to nonionising electromagnetic fields and radiation. R.D. Saunders, C.I. Kowalczuk and Z.J. Sienkiewicz. - III, Radiofrequency and microwave radiation, Chilton, Oxfordshire: National Radiological Protection Board, 1991.

[9] G. Draper, T. Vincent, M. E. Kroll and J. Swa, "Childhood cancer in relation to distance from high voltage power," BMJ, London, 2005.

[10] D. A. Savitz, "Occupational exposure to magnetic fields and brain cancer,"

Department of Epidemiology, University of North Carolina, 2001.

[11] Commission on Radiological Protection, "Schutz vor elektrischen und magnetischen Feldern der elektrischen Energiversorung und -anwendung," Empfehlung der Strahlenschutzkommission, Bohn, 2008.

[12] International commission on non-ionizing radiation protection, "ICNIRP Guidelines for limiting time-varying electric and magnetic fields (1 Hz - 100 kHz)," ICNIRP, Oberschleissheim, 2010.

[13] J. Reddy, An Introduction to the Finite Element Method (Third Edition), McGraw-Hill, 2005.

[14] Wikipedia, "Wikipedia," Wikimedia Foundation, Inc, 29 4 2014. [Online]. Available: http://en.wikipedia.org/wiki/Finite_element_method. [Accessed 39 4 2014].

[15] COMSOL , "COMSOL Multiphysics," COMSOL, 29 04 2014. [Online]. Available: http://www.comsol.com/comsol-multiphysics. [Accessed 29 04 2014].

[16] Narda, "Narda-Sts," 23 4 2014. [Online]. Available: http://www.narda-sts.us/pdf_files/DataSheets/EFA300_DataSheet.pdfl. [Accessed 3 4 2014].

[17] K. C. LLC, "Kallman creations," Kaltman Creations LLC, 23 4 2014. [Online]. Available: http://www.kaltmancreationsllc.com/rf-test-equipment-html/emc-analyzers-html/. [Accessed 23 4 2014].

[18] Narda safety test soulution, "Elkraft NTNU instrumentarkiv," 11 3 2014. [Online]. Available: http://www.elkraft.ntnu.no/elkraft3/instrumentarkiv/n01/narda-efa300b/N01-0017sertfabrikk.pdf. [Accessed 19 5 2014].

[19] Zureks, "Wikipedia," 2009. [Online]. Available: http://en.wikipedia.org/wiki/File:Permeability_by_Zureks.svg. [Accessed 26 Mars 2014].

[20] R. Schmitt, Electromagnetics Explained: A Handbook for Wireless/RF, EMC, and High-speed electronics., 2nd eddition ed., Newnes, 2002.

[21] Siemens AS, "Siemens Norway," SIEMENS, 26 04 2014. [Online]. Available: http://w3.siemens.no/home/no/no/topics/fremtiden-er-elektrisk/Pages/Elektrisk-bilferge.aspx. [Accessed 26 04 2014].

[22] M. Feychting, A. Ahlbom and L. Kheifets, "EMF and health," Annual Reviews Public Health, 2005.

[23] K. K. Shawn , D. R. Wozny and S. B. Baumann, "The Electrical Conductivity of Human Cerebrospinal Fluid at Body Temperature," IEEE, 1997.

[24] J. B. Klauenberg and D. Miklavcic, Radio Frequency Radiation Dosimetry and Its Relationship to the Biological Effects of Electromegnatic Fields., Vol. 82 ed., Dordrecht: Kluwer Academic Publishers, 1998.